DMD Fast Forward. Published on February 21, 2018 as DOI: 10.1124/dmd.117.079277
This article has not been copyedited and formatted. The final version may differ from this version.

Intravital multiphoton microscopy with fluorescent bile salts in rats as an *in vivo* biomarker for hepatobiliary transport inhibition

Ryan, Jennifer, Morgan, Ryan E., Chen, Yuan, Volak, Laurie P., Dunn, Robert T, II, and Dunn, Kenneth W.

Indiana University Medical Center, Indianapolis, IN 46202; Department of Medicine, Division of Nephrology - JR, KWD

Amgen Inc., Thousand Oaks, CA 91320; Department of Comparative Biology and Safety Sciences, Department of Pharmacokinetics and Drug Metabolism - REM, YC, LPV, RTD

DMD Fast Forward. Published on February 21, 2018 as DOI: 10.1124/dmd.117.079277
This article has not been copyedited and formatted. The final version may differ from this version.

Running title - Intravital imaging of Bsep inhibition

Corresponding authors:

Kenneth W. Dunn

kwdunn@iu.edu

Phone (317) 278-0436

Fax (317) 274-8575

Indiana University Medical Center

Department of Medicine, Division of Nephrology

950 W. Walnut St., RII-202B

Indianapolis, Indiana 46202-5116

Ryan E. Morgan

remorgan@amgen.com

Phone (805) 313-5280

Amgen Inc.

Department of Comparative Biology and Safety Sciences

One Amgen Center Dr.

29 – 2 – A

Thousand Oaks, CA 91320

Numbers:

Text pages - 32

Tables - 3

Figures - 13

References - 37

Words in the Abstract - 245

Words in the Introduction - 745

Words in the Discussion – 1293

Non-standard abbreviations

DILI – Drug-induced liver injury
Css – Concentration at steady-state
CGamF - cholylglycyl amidofluorescein
CLF - cholyl-lysyl-fluorescein

DMD Fast Forward. Published on February 21, 2018 as DOI: 10.1124/dmd.117.079277
This article has not been copyedited and formatted. The final version may differ from this version.

Abstract

The bile salt export pump (BSEP) is expressed at the canalicular domain of hepatocytes, where it mediates the elimination of monovalent bile salts into the bile. Inhibition of BSEP is considered a susceptibility factor for drug-induced liver injury (DILI) that often goes undetected during non-clinical testing. Although *in vitro* assays exist for screening BSEP inhibition, a reliable and specific method for confirming Bsep inhibition *in vivo* would be a valuable follow-up to a BSEP screening strategy, helping to put a translatable context around *in vitro* inhibition data, incorporating processes such as metabolism, protein binding, and other exposure properties that are lacking in most *in vitro* BSEP models. Here, we describe studies in which methods of quantitative intravital microscopy were used to identify dose-dependent effects of two known BSEP/Bsep inhibitors, AMG 009 and bosentan, on hepatocellular transport of the fluorescent bile salts, cholylglycyl amidofluorescein (CGamF) and cholyl-lysyl-fluorescein (CLF) in rats. Results of these studies demonstrate that the intravital microscopy approach is capable of detecting Bsep inhibition at drug doses well below those found to increase serum bile acid levels, and also indicate that basolateral efflux transporters play a significant role in preventing cytosolic accumulation of bile acids under conditions of Bsep inhibition in rats. Studies of this kind can both improve our understanding of exposures needed to inhibit Bsep in vivo, but also provide unique insights into drug effects in ways that can improve our ability interpret animal studies for the prediction of human drug hepatotoxicity.

DMD Fast Forward. Published on February 21, 2018 as DOI: 10.1124/dmd.117.079277
This article has not been copyedited and formatted. The final version may differ from this version.

Introduction

Drug-induced liver injury (DILI) is a leading cause of clinical trial failures and post-marketing drug withdrawals. The fact that DILI often goes undetected during non-clinical testing (Olson et al., 2000; Chen et al., 2015) suggests that the mechanisms of drug hepatotoxicity differ between humans and laboratory animals. For example, human hepatotoxicity is strongly associated with drugs that inhibit the bile salt export pump (BSEP), a transporter expressed at the canalicular domain of hepatocytes, with its primary function being the secretion of bile acids into the bile canaliculus (Stieger et al., 2007). In contrast, BSEP inhibitors generally show little or no evidence of liver injury in rodent studies (Fattinger et al., 2001; Funk et al., 2001a; Funk et al., 2001b; Kostrubsky et al., 2003; Kostrubsky et al., 2006; Feng et al., 2009; Morgan et al., 2010; Morgan et al., 2013). Examples of BSEP inhibitors associated with human hepatotoxicity that showed little or no evidence of liver injury during non-clinical testing include: bosentan , AMG 009 and troglitazone (Fattinger et al., 2001; Funk et al., 2001b; Morgan et al., 2013).

There is genetic validation of BSEP as a target for toxicity in humans where mutations in the gene that encodes BSEP (ATP-binding cassette transporter, B11 or *ABCB11*) result in a complete loss of function, and lead to a severe disease phenotype requiring liver transplantation during adolescence (Davit-Spraul et al., 2009). Bsep knockout mice, on the other hand, live a relatively normal life span, with only mild evidence of cholestasis (Wang et al., 2009). Some hypotheses as to the reasons that rodents appear less sensitive to hepatotoxicity due to Bsep inhibition include differences in the bile salt pool, bile salt metabolism, bile salt transporter expression, and others (Wang et al., 2009; Woodhead et al., 2014).

Given the strong association of human hepatotoxicity with drugs that inhibit BSEP and the fact that the liver injury seen in humans often goes undetected during non-clinical testing, a BSEP screening strategy is advised for the early detection of this putative liability. The challenge with such a screening strategy is in translating *in vitro* measures of BSEP inhibition

DMD Fast Forward. Published on February 21, 2018 as DOI: 10.1124/dmd.117.079277
This article has not been copyedited and formatted. The final version may differ from this version.

into predictions of *in vivo* effects. The practice of relating *in vitro* potencies to exposure values, such as concentration at steady state (Css) has been shown to improve the correlation with hepatotoxicity outcome (Dawson et al., 2012; Morgan et al., 2013). However, the typical high-throughput BSEP transport assay utilizes membrane vesicles that over express the transporter, a simplistic system that lacks important components of *in vivo* exposure, such as metabolic capacity, uptake/efflux and protein binding (van Staden et al., 2012). In the absence of a toxicologically relevant *in vivo* model that can recapitulate the BSEP-mediated liver injury seen in humans, an *in vivo* assay of Bsep function could aid in the translation of *in vitro* potencies to an *in vivo* response.

Although rats are not a toxicologically relevant model for Bsep-mediated hepatotoxicity, they can be used to confirm Bsep inhibition *in vivo*. Development of an assay of Bsep function in rats would provide a valuable follow-up to a BSEP screening strategy, helping to put a translatable context around *in vitro* inhibition data, including *in vivo* exposure properties that are lacking in most *in vitro* BSEP models. Such an assay could be used to confirm the exposures needed to achieve *in vivo* BSEP inhibition, and provide a better understanding of the relationship between *in vitro* data and *in vivo* outcome. Knowledge of the exposures needed to achieve *in vivo* Bsep inhibition would improve liver liability assessments by clarifying a margin of safety as compounds are advanced to human testing. Total plasma or serum bile acids have been used to confirm Bsep inhibition in rodents, but this method appears to lack sensitivity as will be shown in this work with AMG 009 and bosentan.

In previous studies, we have demonstrated that quantitative multiphoton microscopy can be used to quantify organic anion and bile acid transport in the liver of living rats at subcellular resolution (Babbey et al., 2012; Ryan et al., 2014; Dunn and Ryan, 2017). Here we extend this approach to assay transporter inhibition in rats, using CGamF and CLF as fluorescent bile salt probes (de Waart et al., 2010; Kruglov et al., 2011). Quantitative intravital microscopy of fluorescent bile salt transport in the liver of living rats was used to identify acute,

dose-dependent effects of AMG 009 and bosentan, two human and rat BSEP/Bsep inhibitors that have been associated with drug-induced liver injury in humans.

Materials and methods

Reagents

Bosentan was purchased from Sequoia Research Products Limited (Pangbourne, UK). AMG 009 was synthesized at Amgen Incorporated (Thousand Oaks, CA). CGamF was purchased from WuXi AppTec (Tianjin, China), and CLF was purchased from Syncom (Groningen, Netherlands). All other reagents were of the highest grade possible, and acquired from readily available commercial vendors.

Dosing solution preparations

Bosentan and AMG 009 dosing solutions suitable for intravenous (IV) administration were prepared. Solutions of bosentan were prepared at 0.6, 2, and 6 mg/mL in 12.5% captisol in distilled water, adjusted to pH 9 using NaOH, for dose levels of 3, 10 and 30 mg/kg, respectively. Solutions of AMG 009 were prepared at 0.6, 2 and 6 mg/mL in distilled water, adjusted to pH 9 using NaOH for dose levels of 3, 10, and 30 mg/kg, respectively.

CGamF powder was dissolved in DMSO (4 mg/50 μL), added to a solution of 0.5 N NaOH, which was then titrated to pH 7 using concentrated HCl to a final concentration of 4 mg/mL. CLF was dissolved in 0.9% saline to a concentration of 10 mg/mL. All experiments conducted for a particular test article were performed using the same batch of CGamF or CLF, with the dose adjusted to accommodate differences in fluorescence between batches so as to ensure hepatocyte labeling in the linear range of the microscope fluorescence detectors.

Animals for intravital microscopy studies

Male Wistar rats (300-400 grams) were purchased from Harlan Laboratories and housed in pairs in the Indiana University School of Medicine Laboratory Animal Resource Center. The rats were maintained on a diet of Teklad 4% mouse/rat diet and water *ad libitum*. An acclimatization interval of at least 4 days was allowed prior to the performance of any experiments. All animal experiments were approved and conducted according to the Institutional Animal Care and Use Committee guidelines of Indiana University, and adhered to the guide for the care and use of animals (National Research Council (U.S.). Committee for the Update of the Guide for the Care and Use of Laboratory Animals. et al., 2011).

Intravital microscopy studies of fluorescent bile salt transport

Fluorescent bile salt transport was characterized using intravital multiphoton microscopy, using an approach similar to that previously applied (Babbey et al., 2012; Ryan et al., 2014), and described in detail (Dunn and Ryan, 2017). Multiphoton microscopy was conducted with an Olympus Fluoview 1000 MPE confocal/multiphoton microscope system mounted on an Olympus IX-81 inverted stand, using an Olympus 25X, NA1.05 water immersion objective, with 830 nm excitation provided by a Spectraphysics MaiTai DeepSee laser. Fluorescence emissions were collected in three non-descanned photomultiplier detectors: blue channel (380-480 nm), green channel (500-550 nm) and red channel (560-650 nm).

Rats were sedated with 5% Isoflurane, weighed and 130 mg/kg Inactin (Sigma Aldrich) was administered intraperitoneally (IP) for anesthesia. During surgery, rats were placed on a heating pad to maintain body temperature, which was monitored using a rectal thermometer. Once anesthetized, a 3 cm x 1.5 cm L-shaped incision was made 1 cm right of ventral midline in the neck. A jugular cannula was then placed using PE 50 tubing, filled with sterile 0.9% saline and attached to a Luer stub adapter and 1 mL syringe, and the neck was sutured with 3-0 black silk sterile suture. At this time, a bolus of Hoechst 33342 (Invitrogen, 2 mg/kg) diluted in 0.9% sterile saline to a total 0.4 mL was injected into the jugular line to label cell nuclei. To expose

the liver for imaging, a ventral 4 cm incision was made across the torso 1 to 2 cm below the middle of the rib cage. A wet (0.9% saline) 2x2 gauze sponge was gently placed below the left lateral liver lobe. The liver was secured to the bottom of a Willco coverslip-bottomed dish (GWST-5040, Warner Instruments, Hamden, Ct) via cyanoacrylate gluing of the gauze below the liver to the plate or by gluing the liver itself to the plate. Sterile 0.9% saline was then placed in the coverslip-bottomed dish to keep the liver moist throughout the imaging session. A small dose of CGamF or CLF was administered IV in order to identify a field of hepatocytes for analysis. Rats were then injected IV with AMG 009, bosentan or vehicle in a volume of 5 mL/kg. The rats were placed ventral side down on the stage of an inverted microscope, with heating pads placed below the rats to warm the stage. A heater was used to warm the objective lens, and another heating pad was placed over each rat prior to imaging. To prevent movement during imaging, the rats' hind legs and the glass-bottom plate were taped securely to the stage. An appropriate field of the liver was identified, and at a time point 20 minutes after administration of test article, a series of image volumes (6 focal planes, spaced at 1 micron apart) were then collected continuously just before and for twelve minutes following IV injection of CGamF or CLF (0.4 – 4.0 mg/kg and 0.5 mg/kg, respectively). A high-resolution mosaic, consisting of 9 contiguous volumes (each consisting of 15 planes, spaced 1 micron apart) was then collected.

Quantitative digital image analysis

Quantitative image analysis was conducted using Metamorph image processing software (Molecular Devices, Downington, PA). To ensure sequential capture of images of the canaliculi despite residual vertical motion of the liver, 3D image volumes were collected at each time-point. Each of these volumes were then projected into a single, maximum-projection image (Babbey et al., 2012; Ryan et al., 2014), which was used for quantitative analysis. This

procedure had the effect of ensuring collection of images of the same set of canaliculi throughout the time series.

Canalicular fluorescence was quantified as follows. In order to eliminate crosstalk of the nuclear Hoechst fluorescence into the CGamF/CLF fluorescence channel, projections of images collected with the blue channel (380-480 nm) were subtracted from the corresponding projected images of the green channel (500-550 nm). A series of binary masks of the canalicular regions were generated by applying a high-pass filter to each time-point projection (subtracting a large-neighborhood (24 pixel square) median filter from each (Maxfield and Dunn, 1990), from which single pixels were then eliminated. The effectiveness of this approach is demonstrated in supplementary data (Supplemental Figure 1). Canalicular fluorescence for each time point was quantified as the integrated green channel signal occurring in the corresponding masked region. Fluorescence measurements were corrected for background by subtracting the mean signal during the 5 time points preceding the appearance of CGamF/CLF in the sinusoids. Net canalicular secretion rates were quantified as the linear slope of the background-corrected measurements obtained from the regions under the canalicular mask during the initial interval of canalicular uptake (typically 1 minute after infusion, ~2 minutes after injection).

In order to quantify mean cytosolic fluorescence, a series of masks of nuclear regions were created by binarizing projections of the images collected in the blue channel (380-480 nm) for each time point. Cytosolic regions were then identified as regions surrounding the nuclear masks, located in two-pixel-wide lines 6 pixels away from the nucleus boundary, after subtraction of the corresponding canalicular mask. Mean cytosolic fluorescence for each time point was quantified as the mean green channel signal occurring in the cytosolic regions. Plotted values were corrected for background by subtracting the mean signal measured in the regions during the 5 time points preceding the appearance of CGamF/CLF in the sinusoids. Cytosolic uptake rates were quantified as the linear slope over the initial interval of cytosolic uptake (starting immediately upon infusion, typically 1 minutes after injection).

Mosaics were assembled from individual volumes by projecting each volume into a single projection image, and then aligning and assembling the projections into a single image using Adobe Photoshop® (Adobe, Mountain View, CA). Canalicular and cytosolic fluorescence in the mosaics were quantified as described above, and standardized to a common field size to compensate for small differences in the size of the resulting mosaics.

Measurement of serum total bile acids from rats exposed to AMG 009 or bosentan

Biochemical analyses of the effects of drugs on serum bile acid levels were conducted using male Sprague-Dawley rats which, like the Wistar rats used in the microscopy studies, have been extensively used in Bsep inhibitor studies (Fattinger et al., 2001; Kostrubsky et al., 2003; Leslie et al., 2007; Morgan et al., 2013) and have been found to show a similar sensitivity to bosentan (Fouassier et al., 2002). Rats approximately 10 weeks of age were purchased from Charles River Laboratories (Wilmington, Massachusetts) and allowed at least one week to acclimate. All animals were group housed (2 or 3 per cage) at an AAALAC, Intl-accredited facility in nonsterile, ventilated microisolator housing. The research protocols were approved by the Institutional Animal Care and Use Committee. Animals were given ad libitum access to pelleted feed and purified, municipal water. The light:dark cycle was 12:12 hr with controlled temperature and humidity. Animals were given access to enrichment opportunities. Animals were fasted 2 – 3 hrs prior to the administration of a single IV dose of either AMG 009 (Amgen study 111327) or bosentan (Amgen study 118507), and food returned following the final bleed prior to the 24 hr time point (2 – 6 hr post dose). Animals were again fasted 2 – 3 hrs prior to the terminal 24 hr bleed.

The formulations and dosing volumes were as described under the dosing solution preparations section. For the Amgen serum total bile acid studies, 0, 10, 30 and 100 mg/kg dose levels were evaluated for AMG 009 or bosentan. For the AMG 009 study, 6 animals were assigned to each dose group where the first 3 animals in each group were bled at 5, 30, 60, and

360 min post dose (terminal bleed at 360 min post dose), and the second 3 animals in each group were bled at 15, 45, 120, and 1440 min post dose. Plasma was collected for exposure analysis at each time point, and serum collected for total bile acid analysis. Total bile acids were measured using an enzymatic, colorimetric assay for total bile acids from BioQuant (San Diego, CA, catalog number BQ092A-EALD) and a Tecan Safire plate reader (540 nm wavelength). In the bosentan studies, there were 10 animals per dose group. The first 5 animals in each group were bled at 5, 30, 120 and 1440 min post dose, and the second 5 animals per dose group were bled at 15, 60, 360, and 1440 min post dose. Plasma was collected for exposure analysis at each time point, and serum collected for total bile acid analysis. Total bile acids were measured using the BioQuant assay described above; however, the analysis was performed on a Beckman Coulter AU400 chemistry analyzer.

Analysis of rat plasma samples

In the intravital imaging studies conducted at Indiana University Medical Center, plasma samples were collected in lithium heparin tubes 50 min post IV dose of AMG 009 or bosentan, stored at approximately 70˚C, and shipped on dry ice to Amgen for exposure analysis. Briefly, plasma was analyzed by liquid chromatography mass spectrometry using multiple reaction monitoring (MRM) in positive ionization mode. The lower limit of quantitation (LLOQ) for both AMG 009 and bosentan in the assay was 100 µg/L. Verapamil was used as an internal standard. The bioanalytical and toxicokinetic analyses were performed in Watson LIMS.

To estimate the maximum concentration (C_{max}) achieved following a single, bolus IV dose of AMG 009 or bosentan in male rats from the 50 min post dose samples collected during the intravital studies, exposure data from previously conducted IV studies (Amgen studies 111327 and 118507) were compared to the intravital exposure values. For the previous AMG 009 study (111327), the plasma concentrations for individual animals at the 45 min time point were plotted against C_{max}. In this study, three animals per dose group were bled at 15, 45, 120

DMD Fast Forward. Published on February 21, 2018 as DOI: 10.1124/dmd.117.079277
This article has not been copyedited and formatted. The final version may differ from this version.

and 1440 min post dose or at 5, 30, 30, and 360 min post dose. Linear regression of the plasma concentration at 45 min post dose versus C_{max} was performed, resulting in the equation y = 0.571x, where "y" is the plasma concentration and x is the estimated Cmax. The intravital plasma concentrations at 50 min post dose were then substituted for "y" to generate an estimated C_{max}. Similarly, for the previous bosentan study (118507), 5 animals per dose group were bled at 5, 30, 120 and 1440 min post dose, or at 15, 60, 360 and 1440 min post dose. Linear regression of the plasma concentrations at the 30 and 60 min time points versus C_{max} was performed, resulting in the equation y = 0.710x, where "y" is the plasma concentration and x is the estimated C_{max}. The intravital plasma concentrations at 50 min post dose for the bosentan-treated animals were then substituted for "y" to establish an estimated C_{max}.

In vitro functional transport assessments in membrane vesicles over-expressing rat Bsep or Mrp2

Inverted membrane vesicles created from Sf9 insect cells over-expressing rat Bsep or Mrp2 (catalog numbers GM0006 and GM0002, respectively) were purchased from Life Technologies (Grand Island, NY). Radioactive substrates for the membrane vesicle assays, ^{3}H-taurocholate (^{3}H-T) for Bsep and ^{3}H-estradiol-17β-D-glucuronide (^{3}H-$E_2$17βG) for Mrp2, were purchased from Perkin Elmer (Waltham, MA). All other reagents and buffers for the membrane vesicle assays were of the highest grade possible and were exactly as described in van Staden et al (van Staden et al., 2012). The transporter methods and data analyses performed in the present work were also exactly as described in van Staden et al, 2012, however the membrane vesicles were for the rat versions of Bsep and Mrp2. Briefly, rat Bsep (25 µg membrane vesicle protein per reaction) or Mrp2 (50 µg membrane vesicle protein per reaction) membrane vesicles were incubated with a radiolabeled substrate in the presence or absence of 4 mM ATP. The absence of ATP served as the negative control, and resulting radioactivity when exposed to vehicle alone (1.3% DMSO) was considered background or noise. The with-ATP controls and

DMD Fast Forward. Published on February 21, 2018 as DOI: 10.1124/dmd.117.079277
This article has not been copyedited and formatted. The final version may differ from this version.

1.3% DMSO represented true signal. For the rat Mrp2 assay, 2 mM GSH was added to the reaction. The Bsep assay was performed at room temperature, with an incubation time of 15 – 20 min. The Mrp2 assay was performed at 37°C, with an incubation time of 20 min. AMG 009 or bosentan were evaluated at 10 concentrations, diluted in 1/3 increments, spanning 0 – 133 μM. Non-linear regression analysis was performed, and IC_{50} values generated as an estimate of potency as described previously (Morgan et al., 2010; van Staden et al., 2012).

Additional experiments were conducted to evaluate the *in vitro* transport of CGamF or CLF in rat Bsep or Mrp2 membrane vesicles. These experiments were conducted exactly as described above, however no radioactive substrates were added to the reactions. The transport of CGamF or CLF were tested at 0 – 133 μM, 10 concentrations per fluorescent probe, diluted in 1/3 increments, and in the presence of 4 mM ATP. As performed in the radioactivity-based assays described above, with or without ATP controls represented maximum signal or background fluorescence, respectively. After the filter plates were washed four times with cold washing buffer and air dried, 100 μL of 0.1 N NaOH was used to lyse the membrane vesicles. The lysates were collected via vacuum filtration into collection plates, and the fluorescence measured at an excitation of 490 nm, and an emission of 525 nm using a Tecan Infinite plate reader.

Figure preparation

Quantitative analysis was conducted on raw image data, but micrograph images were both contrast enhanced (resetting minimum and maximal values, and adjusting gamma to 1.2) and smoothed, using a Gaussian filter. In color images, the visibility of Hoechst-labeled nuclei was enhanced by selectively adjusting the hue, saturation and lightness of the blue channel. In all cases, images to be compared were processed identically to one another and in such a way that the processing preserved the visibility of both the dim and bright structures of the original

image. Images were processed, assembled into figures and annotated using Adobe Photoshop®). Graphics were produced and summary statistics obtained using Kaleidagraph (Synergy Software, Reading, PA).

Preparation of videos

Mpg videos were prepared using the TMPGEnc 2.5 video encoder (*http://www.tmpgenc.net/)*, from uncompressed AVI files prepared in Metamorph.

Results

Intravital microscopy of CGamF hepatocellular transport in rats

The metabolism and transport of CGamF have been previously shown to be similar to that of native bile salts in rats (Holzinger et al., 1997) and in perfused rat livers (Holzinger et al., 1998). Studies of transfected cells demonstrate that CGamF is a substrate for human NTCP and BSEP (Mita et al., 2006) and for rat Ntcp (Boyer et al., 1994). Studies of cultured rat hepatocytes have demonstrated that Bsep expression is required for CGamF secretion (Kruglov et al., 2011). Our studies of inverted membrane vesicles created from Sf9 insect cells over-expressing rat Bsep or Mrp2 demonstrate that CGamF is transported by both Bsep and, to a lesser extent, Mrp2 in an ATP-dependent manner (Supplemental Figure 2).

Figure 1 shows a time series of multiphoton fluorescence excitation images collected from a 364x364 micron region of the liver of a living rat following intravenous injection of CGamF. Nuclei were labeled (blue) by IV injection of Hoechst 33342 30 minutes prior to imaging. These images demonstrate that CGamF (green fluorescence) is rapidly transported from sinusoids to bile canaliculi, with detectible fluorescence appearing in canaliculi within a minute of infusion, and subsequently increasing in intensity over the next 3 minutes.

DMD Fast Forward. Published on February 21, 2018 as DOI: 10.1124/dmd.117.079277
This article has not been copyedited and formatted. The final version may differ from this version.

Intravital microscopy of the effects of AMG 009 on CGamF hepatocellular transport in rats

In order to evaluate the effect of AMG 009 on hepatic bile salt transport, the same approach was used to characterize CGamF transport in rats 20 minutes after IV administration of 3, 10 or 30 mg/kg AMG 009 or vehicle. Figure 2A shows that detectible amounts of CGamF are found in canaliculi within 90 seconds of infusion in a vehicle-treated rat, subsequently increasing in brightness over the next 3.5 minutes. In contrast, transport of CGamF into canaliculi is slowed or blocked completely in rats treated with either 10 or 30 mg/kg AMG 009, respectively. The inhibitory effect of AMG 009 on CGamF transport is also demonstrated in the complete 8 minute series of images shown in an accompanying video (Supplemental Video1), which shows that the rapid canalicular transport observed in a vehicle-treated rat is completely absent in a rat treated with 30 mg/kg AMG 009.

These studies were repeated for 3 rats per treatment, and digital image analysis was used to quantify canalicular fluorescence over time (Figures 3A-D). The results of these studies show that; canalicular transport of CGamF was essentially blocked in rats treated with 10 or 30 mg/kg, and in two of three rats treated with 3 mg/kg AMG 009. It is uncertain why one animal in the 3 mg/kg group did not respond as the AMG 009 exposure for this animal was similar to that achieved in the other two. Rates of net secretion, measured as the linear rate of change in canalicular fluorescence during the initial secretion period, demonstrate that the rate of canalicular transport of CGamF is significantly reduced 20 minutes after treatment with 10 or 30 mg/kg AMG 009 (Figure 3E).

In order to evaluate the effects of AMG 009 on CGamF hepatocellular uptake, we measured the change in mean cytosolic fluorescence over time for each animal. These quantifications showed similar initial rates of increase for all treatment conditions, although the peak cytosolic fluorescence varied between and within each treatment (Figures 4A-D). Quantification of uptake rates (measured as the linear rate of change in mean cytosolic

fluorescence during the initial uptake period) showed that AMG 009 had no significant effect on the CGamF uptake rate (Figure 4E). These results support the conclusion that AMG 009 inhibits CGamF transport into the bile by blocking canalicular secretion.

In the presence of unimpeded uptake (i.e. Ntcp inhibition), one would expect that AMG 009 doses that block secretion would induce significant cytosolic accumulation of CGamF. Surprisingly, the measurements of cytosolic fluorescence shown in Figures 4A-D indicate no such effect. Quantifications of cytosolic CGamF exposure, (measured as cumulative cytosolic fluorescence over the period from 6-11 minutes after injection), likewise indicate that inhibition of canalicular CGamF secretion by AMG 009 was not accompanied by a corresponding increase in cytosolic CGamF levels (Figure 4F).

Although it was not possible to characterize the kinetics in more than one field for each animal, the behaviors of the single fields were essentially reproduced in 9-field mosaics that were collected from the surrounding regions 12-15 minutes after probe administration (Figure 2B). These mosaics, representing ~1 mm by 1 mm regions encompassing several lobules, consistently demonstrated that the behaviors of the single fields used for kinetic analysis were representative of larger regions, and also demonstrated that their function was not significantly impacted by repeated imaging. Quantifications of total canalicular fluorescence in these mosaics supported the kinetic analyses, demonstrating that AMG 009 significantly reduced the total amount of canalicular CGamF at doses of 10 and 30 mg/kg, but had no effect on mean levels of CGamF fluorescence in hepatocyte cytosols (Table 1).

Intravital microscopy of the effects of AMG 009 on CLF hepatocellular transport in rats

The effects of AMG 009 on hepatic transport were also evaluated using the fluorescent probe cholyl-lysyl-fluorescein (CLF), a fluorescent probe that is frequently used to assay hepatocellular transport (Swift et al., 2010; Letzsch et al., 2015). While studies of transfected cells suggest that biliary secretion of CLF is mediated by MRP2 in humans (de Waart et al.,

2010), studies of wild-type and Mrp2-deficient TR- rats indicate that CLF secretion is mediated by Bsep in rats (Mills et al., 1997; Mills et al., 1999). Our studies of inverted membrane vesicles created from Sf9 insect cells over-expressing rat Bsep or Mrp2 demonstrate that CLF is transported by both Bsep and Mrp2 in an ATP-dependent manner *in vitro* (Supplemental Figure 2).

Similar to results obtained with CGamF, treatment of rats with 30 mg/kg AMG 009 blocked secretion of CLF into bile canaliculi (Figures 5, 6A), significantly reducing the rate of net secretion (Figure 6B, Table 1). The effect of AMG 009 was demonstrated in the complete 8 minute series of images shown in an accompanying video (Supplemental Video2), which shows that, like CGamF, the rapid canalicular transport of CLF observed in a vehicle-treated rat is completely absent in a rat treated with 30 mg/kg AMG 009. Whereas AMG 009 had no effect on CGamF uptake, treatment of rats with 30 mg/kg AMG 009 significantly inhibited CLF uptake, reducing the initial rate of uptake by more than 50% in (Figures 6C and 6D). Although the kinetics of cytosolic CLF fluorescence suggest that AMG 009 increases cytosolic exposure to CLF, differences in cumulative cytosolic fluorescence, measured from 6-11 minutes after infusion, were not statistically significant (Table 1).

Effects of AMG 009 on plasma bile acid levels

Serum samples were collected from rats over a 24 hr period following IV injection of vehicle, 10, 30 or 100 mg/kg AMG 009 and analyzed for total bile acids. As shown in Figure 7, treatment of animals with 10 and 30 mg/kg had no detectible effect on serum bile acid levels, whereas a dose of 100 mg/kg resulted in a statistically significant elevation of total serum bile acids from 5 to 120 min post dose. Bile acids then returned to vehicle control values by 360 and 1440 min post dose.

Intravital microscopy of the effects of bosentan on CGamF hepatocellular transport in rats

Similar studies were conducted in rats treated with 3, 10 or 30 mg/kg bosentan, another Bsep inhibitor that has been associated with liver injury in humans (Fattinger et al., 2001). The effects of bosentan on CGamF canalicular secretion were similar to those observed in the studies with AMG 009 (Figures 8A and 9), with significant decreases in the rates of net secretion apparent at both 10 and 30 mg/kg doses (Figure 9 E). This inhibitory effect is also demonstrated in the complete 8 minute series of images shown in an accompanying video (Supplemental Video3), which shows that the rapid canalicular transport observed in a vehicle-treated rat is significantly inhibited in a rat treated with 30 mg/kg bosentan. Evaluations of the 9-field mosaics (Figure 8B) indicated that the results obtained in the kinetic studies of individual fields were generally representative; total canalicular fluorescence in these large regions was reduced approximately two fold in rats treated with 10 or 30 mg/kg bosentan, although the differences were not statistically significant (Table 1).

Previous studies have demonstrated that bosentan inhibits Na-dependent taurocholate uptake by suspended rat hepatocytes (Leslie et al., 2007). Consistent with these studies, our data indicated a dose-dependent inhibition of CGamF uptake by bosentan (Figures 10A-E), although the differences in rates were statistically significant only at a dose of 30 mg/kg. As with AMG 009, bosentan had no effect on cytosolic levels of CGamF, quantified either as cytosolic exposure from 6-11 minutes after injection (Figure 10F), or as mean cytosolic fluorescence in the 9-field mosaics (Table 1).

Intravital microscopy of the effects of bosentan on hepatocyte transport of CLF in rats

The effects of bosentan on CLF transport essentially reproduce the effects observed on CGamF transport. As with CGamF, CLF secretion was significantly reduced in rats treated with 30 mg/kg bosentan; the rate of net secretion was reduced more than 3-fold (Figures 11, 12A and 12B, Table 1). The effect of bosentan on CLF secretion is also demonstrated in the 8 minute series of images shown in an accompanying video (Supplemental Video4). The effect of

DMD Fast Forward. Published on February 21, 2018 as DOI: 10.1124/dmd.117.079277
This article has not been copyedited and formatted. The final version may differ from this version.

bosentan on hepatocyte uptake of CLF likewise reproduces the results obtained with CGamF; although the effect was somewhat larger (3-fold, Figures 12C and D). Quantifications of cumulative cytosolic fluorescence indicate that bosentan induced a small, statistically insignificant increase in cytosolic exposure to CLF (Table 1), consistent with results obtained with CGamF.

Effects of bosentan on plasma bile acid levels

Similar to AMG 009, 100 mg/kg IV administration of bosentan to rats resulted in a statistically significant elevation of total serum bile acids from 5 to 120 min post dose, and bile acid levels returned to vehicle control values by 360 min post dose (Figure 13). Animals receiving an IV dose of 30 mg/kg bosentan had elevated levels of serum bile acids that were statistically significant at 5, 15, and 60 min post dose, returning to control levels by 360 min. The dose level of 10 mg/kg bosentan had no effect on serum bile acid levels relative to vehicle controls throughout the time course.

Relative sensitivity of the intravital microscopy assay relative to measurement of serum bile acid levels

The studies described above demonstrate that whereas the intravital microscopy assay was capable of detecting inhibitory effects of AMG 009 on CGamF secretion at doses as low as 10 mg/kg, serum bile acids were not increased at doses below 100 mg/kg. Likewise, bosentan was found to significantly inhibit CGamF secretion at doses as low as 10 mg/kg, whereas increases in serum bile acids were not apparent at doses below 30 mg/kg.

In order to express these differences in terms of estimated C_{max}/IC_{50} ratios for Bsep and Mrp2, transport studies were conducted to measure IC_{50} concentrations in inverted membrane vesicles expressing either Bsep or Mrp2. These studies (described in Methods) determined that AMG 009 inhibited Bsep with an IC_{50} of 23 μM and inhibited Mrp2 with an IC_{50} of 41 μM. In

DMD Fast Forward. Published on February 21, 2018 as DOI: 10.1124/dmd.117.079277
This article has not been copyedited and formatted. The final version may differ from this version.

contrast, bosentan inhibited Bsep (IC_{50} = 41 μM) but not Mrp2 (IC_{50} > 133 μM, the highest concentration tested). Since it was not possible to perform serial plasma sampling during the imaging procedures, C_{max} values for the intravital microscopy studies were estimated based upon plasma drug levels measured 50 minute after drug administration. Using relationships between C_{max} and plasma concentrations obtained previously (Supplemental Figure 3), plasma concentrations obtained for each intravital microscopy study were converted to C_{max} values by linear regression. These results are presented in Table 2, which also lists the measured plasma drug exposures for each animal.

When evaluated in terms of the estimated C_{max}/IC_{50} ratios for Bsep and Mrp2, the intravital microscopy assay showed approximately 14-fold greater sensitivity to the effects of AMG 009 as compared with measurements of serum total bile acids (Table 3). Whereas significant effects of AMG 009 on serum bile acid levels were not observed at estimated C_{max}/IC_{50} ratios below 44 and 25 (for Bsep and Mrp2, respectively), the intravital microscopy assay detected significant effects on CGamF secretion at estimated C_{max}/IC_{50} ratios of 3.2 and 1.8, respectively. Intravital CLF transport studies were likewise more sensitive than measurements of serum bile acids, detecting significant effects at an estimated C_{max}/IC_{50} ratio of 20 (the only dose tested). The intravital microscopy assay was also more sensitive for detecting the effects of bosentan. Whereas significant effects of bosentan on serum bile acid levels were not observed at C_{max}/ Bsep IC_{50} ratios below 4.6, the intravital microscopy assay detected significant effects on CGamF secretion at a C_{max}/IC_{50} ratio of 0.9.

Discussion

Here we describe studies in which quantitative intravital microscopy was used to characterize hepatic transport of fluorescent bile salts CGamF and CLF, identifying dose-dependent effects of AMG 009 and bosentan on Bsep activity, two compounds associated with

liver injury in humans. While these fluorescent probes cannot represent the full spectrum of bile acids, both have been thoroughly characterized as probes of hepatic transport in rats (Boyer et al., 1994; Holzinger et al., 1997; Mills et al., 1997; Holzinger et al., 1998; Mills et al., 1999; Kruglov et al., 2011), whose transport is mediated by Bsep (Boyer et al., 1994; Mills et al., 1997; Mills et al., 1999; Kruglov et al., 2011)(Supplementary Figure 2), indicating their appropriateness for studies of Bsep function. Although CGamF has been extensively used to characterize bile salt transport *in vitro* (Maglova et al., 1995; Cantz et al., 2000; Ye et al., 2008; Kruglov et al., 2011), the studies described here represent the first use of CGamF for intravital microscopic studies of bile acid transport, and the first demonstrations of dose-dependent effects of drugs on the individual steps of hepatocyte bile salt transport *in vivo*.

Quantitative analyses of images collected from living rats over time after injection of CGamF demonstrated that intravital microscopy was capable of detecting profound effects on canalicular secretion at drug dosages well below those that alter levels of serum bile acids. Whereas significant elevations of serum bile acids were not observed at doses of AMG 009 below 100 mg/kg, intravital microscopy studies demonstrated that canalicular secretion of CGamF was essentially blocked in rats treated with either 10 or 30 mg/kg, and in two out of three rats treated with 3 mg/kg. Whereas serum bile acid elevations were not observed at bosentan doses below 30 mg/kg, intravital microscopy studies detected significant decreases in canalicular secretion of CGamF at doses of 10 mg/kg.

The effects of AMG 009 and bosentan on CGamF secretion were essentially reproduced using CLF, suggesting that CLF is another useful fluorescent bile acid probe, despite its lower activity as a Bsep substrate relative to CGamF (Supplemental Figure 2). Consistent with previous studies of Mrp2-deficient TR- rats (Mills et al., 1997; Mills et al., 1999), our intravital studies, which show that bosentan, an inhibitor of Bsep but not Mrp2, reduces CLF transport nearly 3-fold, suggest that *in vivo* transport of CLF is largely mediated by Bsep in rats.

The capability to resolve the hepatocyte cytosol and bile canaliculi gives intravital microscopy the unique capability to dissect hepatic transport into the component processes of hepatocyte uptake and canalicular secretion, and thus distinguish transport disruptions that could have profoundly different consequences. These studies demonstrated that AMG 009 had no effect on the rate of CGamF uptake at any dose, but reduced the rate of uptake at a dose of 30 mg/kg. In contrast, that bosentan significantly reduced the rate of uptake of both CGamF and CLF at a dose of 30 mg/kg. The basis of these different results is unclear, but may reflect differences in the uptake mechanisms of CGamF and CLF.

The most striking result of these studies is that dosages of AMG009 and bosentan sufficient to essentially block canalicular secretion did not increase cytosolic levels of CGamF and induced only modest, statistically insignificant increases in cytosolic levels of CLF. Insofar as the hepatotoxicity of Bsep inhibitors is believed to be mediated by the cytosolic accumulation of bile acids (Kostrubsky et al., 2003; Morgan et al., 2010; Dawson et al., 2012), the lack of accumulation observed in our studies may explain the absence of liver injury in rats treated with AMG009 or bosentan. More significant to the issue of drug development, our measurements of the effects of these drugs on uptake and secretion suggest potential mechanisms preventing bile acid accumulation in rats. As described below, differences in the role of these mechanisms in humans and rats may explain why these drugs cause liver injury in humans but not in rats.

The lack of cytosolic accumulation in bosentan-treated rats may reflect the fact that bosentan not only inhibited canalicular secretion, but also inhibited uptake of CGamF and CLF. The effect on uptake is consistent with *in vitro* studies showing that bosentan inhibits rat Ntcp (Leslie et al., 2007). These same studies demonstrated that rat Ntcp is inhibited by bosentan at doses >30-fold lower than human NTCP, a difference that the authors suggest may underlie the observation that bosentan hepatotoxicity is observed in humans, but not in rats. According to this model, the accumulation of toxic bile acids that might occur upon Bsep inhibition in humans may be prevented in rats by a concomitant inhibition of bile acid uptake. The intravital

microscopy studies presented here provide crucial support for this model, establishing that bosentan inhibits both canalicular uptake and secretion *in vivo*, while failing to increase cytosolic levels of fluorescent bile acids even in the absence of canalicular secretion.

The absence of cytosolic accumulation of CGamF in rats treated with doses of AMG009 sufficient to block canalicular secretion cannot be explained by effects on uptake, which we found to be completely unaffected. The lack of accumulation despite unimpeded uptake strongly suggests that the cytosolic accumulation of CGamF may be modulated by the activities of basolateral efflux transporters, such as Mrp3 or Mrp4. This interpretation is consistent with the results of studies demonstrating that taurocholate is secreted predominantly from the basolateral side of cultured rat hepatocytes (Jemnitz et al., 2010). The authors of this study suggest that basolateral secretion protects rat hepatocytes from the accumulation of Bsep substrates under conditions of Bsep inhibition. Based upon the observation that Bsep inhibition increased cytosolic taurocholate levels in human hepatocytes 25 fold beyond those observed in rat hepatocytes, they also speculated that the enhanced hepatotoxicity of Bsep inhibitors in humans may be based upon the relative weakness of this pathway in human hepatocytes. The importance of this pathway in human hepatotoxicity of BSEP inhibitors was demonstrated in an analysis of more than 600 drugs, which showed that the ability to predict human liver injury could be increased by considering effects on both BSEP and MRP proteins (Morgan et al., 2013). The unique window into hepatocellular transport provided by the intravital studies presented here provide critical support for this model, demonstrating that AMG009 blocks canalicular secretion without increasing cytosolic levels of CGamF, despite ongoing uptake, strongly suggesting the importance of the basolateral secretory pathway in mediating the effects of Bsep inhibitors.

A fundamental problem in pharmaceutical development is that many drugs identified as safe in studies of laboratory animals are subsequently found to induce liver injury in humans. The studies of Leslie and Jemnitz described above provide a template for how a thorough

understanding of the effects of Bsep inhibitors on all uptake and secretory pathways may be critical to using interpreting animal studies with respect to human safety. To the degree that the human hepatotoxicity of a BSEP inhibitor is mediated by the cytosolic accumulation of bile acids, determining the differential effects on the drug on human and rat NTCP will be crucial to identifying drugs whose human hepatotoxicity will not be predicted in studies of rats. The hepatotoxicity of BSEP inhibitors may be generally modulated in rats by a basolateral secretory pathway whose reduced activity in humans may lead to unanticipated human hepatotoxicity. Predictions of human hepatotoxicity will thus depend upon evaluation of the effects of Bsep inhibitors on the activity of both human and rat MRP transporters. The studies presented here demonstrate how quantitative intravital microscopy can be used to provide crucial *in vivo* validation of these models, establishing whether in the complex in vivo setting of protein binding, metabolism and clearance the candidate drug has the expected effects on uptake, canalicular secretion and, crucially, cytosolic accumulation of bile acids.

Acknowledgments

We would like to thank Claudio Schteingart for helpful advice on the preparation of CGamF solutions. Studies were supported by funding from Amgen. Microscopy studies were conducted at the Indiana Center for Biological Microscopy.

Author contributions

Participated in research design: Morgan and K. Dunn

Conducted experiments: Ryan, Morgan, Chen and Volak

Performed data analysis: K. Dunn, Morgan, Ryan and Volak

Wrote or contributed to manuscript writing: K. Dunn, Morgan, Ryan, Chen, Volak, R. Dunn

References

Babbey CM, Ryan JC, Gill EM, Ghabril MS, Burch CR, Paulman A, and Dunn KW (2012) Quantitative intravital microscopy of hepatic transport. *Intravital* **1:**10.

Boyer JL, Ng OC, Ananthanarayanan M, Hofmann AF, Schteingart CD, Hagenbuch B, Stieger B, and Meier PJ (1994) Expression and characterization of a functional rat liver Na+ bile acid cotransport system in COS-7 cells. *The American journal of physiology* **266:**G382-387.

Cantz T, Nies AT, Brom M, Hofmann AF, and Keppler D (2000) MRP2, a human conjugate export pump, is present and transports fluo 3 into apical vacuoles of Hep G2 cells. *American journal of physiology Gastrointestinal and liver physiology* **278:**G522-531.

Chen M, Suzuki A, Borlak J, Andrade RJ, and Lucena MI (2015) Drug-induced liver injury: Interactions between drug properties and host factors. *Journal of hepatology* **63:**503-514.

Davit-Spraul A, Gonzales E, Baussan C, and Jacquemin E (2009) Progressive familial intrahepatic cholestasis. *Orphanet J Rare Dis* **4:**1.

Dawson S, Stahl S, Paul N, Barber J, and Kenna JG (2012) In vitro inhibition of the bile salt export pump correlates with risk of cholestatic drug-induced liver injury in humans. *Drug metabolism and disposition: the biological fate of chemicals* **40:**130-138.

de Waart DR, Hausler S, Vlaming ML, Kunne C, Hanggi E, Gruss HJ, Oude Elferink RP, and Stieger B (2010) Hepatic transport mechanisms of cholyl-L-lysyl-fluorescein. *The Journal of pharmacology and experimental therapeutics* **334:**78-86.

Dunn KW and Ryan JC (2017) Using quantitative intravital multiphoton microscopy to dissect hepatic transport in rats. *Methods*.

Fattinger K, Funk C, Pantze M, Weber C, Reichen J, Stieger B, and Meier PJ (2001) The endothelin antagonist bosentan inhibits the canalicular bile salt export pump: a potential mechanism for hepatic adverse reactions. *Clinical pharmacology and therapeutics* **69:**223-231.

Feng B, Xu JJ, Bi YA, Mireles R, Davidson R, Duignan DB, Campbell S, Kostrubsky VE, Dunn MC, Smith AR, and Wang HF (2009) Role of hepatic transporters in the disposition and hepatotoxicity of a HER2 tyrosine kinase inhibitor CP-724,714. *Toxicological sciences : an official journal of the Society of Toxicology* **108:**492-500.

Fouassier L, Kinnman N, Lefevre G, Lasnier E, Rey C, Poupon R, Elferink RP, and Housset C (2002) Contribution of mrp2 in alterations of canalicular bile formation by the endothelin antagonist bosentan. *Journal of hepatology* **37:**184-191.

Funk C, Pantze M, Jehle L, Ponelle C, Scheuermann G, Lazendic M, and Gasser R (2001a) Troglitazone-induced intrahepatic cholestasis by an interference with the hepatobiliary export of bile acids in male and female rats. Correlation with the gender difference in troglitazone sulfate formation and the inhibition of the canalicular bile salt export pump (Bsep) by troglitazone and troglitazone sulfate. *Toxicology* **167:**83-98.

Funk C, Ponelle C, Scheuermann G, and Pantze M (2001b) Cholestatic potential of troglitazone as a possible factor contributing to troglitazone-induced hepatotoxicity: in vivo and in vitro interaction at the canalicular bile salt export pump (Bsep) in the rat. *Molecular pharmacology* **59:**627-635.

Holzinger F, Schteingart CD, Ton-Nu HT, Cerre C, Steinbach JH, Yeh HZ, and Hofmann AF (1998) Transport of fluorescent bile acids by the isolated perfused rat liver: kinetics, sequestration, and mobilization. *Hepatology (Baltimore, Md* **28:**510-520.

Holzinger F, Schteingart CD, Ton-Nu HT, Eming SA, Monte MJ, Hagey LR, and Hofmann AF (1997) Fluorescent bile acid derivatives: relationship between chemical structure and hepatic and intestinal transport in the rat. *Hepatology (Baltimore, Md* **26:**1263-1271.

Jemnitz K, Veres Z, and Vereczkey L (2010) Contribution of high basolateral bile salt efflux to the lack of hepatotoxicity in rat in response to drugs inducing cholestasis in human. *Toxicological sciences : an official journal of the Society of Toxicology* **115:**80-88.

Kostrubsky SE, Strom SC, Kalgutkar AS, Kulkarni S, Atherton J, Mireles R, Feng B, Kubik R, Hanson J, Urda E, and Mutlib AE (2006) Inhibition of hepatobiliary transport as a predictive method for clinical hepatotoxicity of nefazodone. *Toxicological sciences : an official journal of the Society of Toxicology* **90:**451-459.

Kostrubsky VE, Strom SC, Hanson J, Urda E, Rose K, Burliegh J, Zocharski P, Cai H, Sinclair JF, and Sahi J (2003) Evaluation of hepatotoxic potential of drugs by inhibition of bile-acid transport in cultured primary human hepatocytes and intact rats. *Toxicological sciences : an official journal of the Society of Toxicology* **76:**220-228.

Kruglov EA, Gautam S, Guerra MT, and Nathanson MH (2011) Type 2 inositol 1,4,5-trisphosphate receptor modulates bile salt export pump activity in rat hepatocytes. *Hepatology (Baltimore, Md* **54:**1790-1799.

Leslie EM, Watkins PB, Kim RB, and Brouwer KL (2007) Differential inhibition of rat and human Na+-dependent taurocholate cotransporting polypeptide (NTCP/SLC10A1)by bosentan: a mechanism for species differences in hepatotoxicity. *The Journal of pharmacology and experimental therapeutics* **321:**1170-1178.

Letzsch S, Boettcher K, Kelm J, and Messner S (2015) Quantifying Efflux Activity in 3D Liver Spheroids. *Genetic Engineering and Biotechnology News* **35:**2.

Maglova LM, Jackson AM, Meng XJ, Carruth MW, Schteingart CD, Ton-Nu HT, Hofmann AF, and Weinman SA (1995) Transport characteristics of three fluorescent conjugated bile acid analogs in isolated rat hepatocytes and couplets. *Hepatology (Baltimore, Md* **22:**637-647.

Maxfield FR and Dunn KW (1990) Studies of endocytosis using image intensification fluorescence microscopy and digital image analysis, in: *Optical Microscopy for Biology* (Jacobsen BHaK ed), pp 357-371, Alan Liss, New York.

Mills CO, Milkiewicz P, Muller M, Roma MG, Havinga R, Coleman R, Kuipers F, Jansen PL, and Elias E (1999) Different pathways of canalicular secretion of sulfated and non-sulfated fluorescent bile acids: a study in isolated hepatocyte couplets and TR- rats. *Journal of hepatology* **31:**678-684.

Mills CO, Milkiewicz P, Saraswat V, and Elias E (1997) Cholyllysyl fluroscein and related lysyl fluorescein conjugated bile acid analogues. *Yale J Biol Med* **70:**447-457.

Mita S, Suzuki H, Akita H, Hayashi H, Onuki R, Hofmann AF, and Sugiyama Y (2006) Inhibition of bile acid transport across Na+/taurocholate cotransporting polypeptide (SLC10A1) and bile salt export pump (ABCB 11)-coexpressing LLC-PK1 cells by cholestasis-inducing drugs. *Drug metabolism and disposition: the biological fate of chemicals* **34:**1575-1581.

Morgan RE, Trauner M, van Staden CJ, Lee PH, Ramachandran B, Eschenberg M, Afshari CA, Qualls CW, Jr., Lightfoot-Dunn R, and Hamadeh HK (2010) Interference with bile salt export pump function is a susceptibility factor for human liver injury in drug development. *Toxicological sciences : an official journal of the Society of Toxicology* **118:**485-500.

Morgan RE, van Staden CJ, Chen Y, Kalyanaraman N, Kalanzi J, Dunn RT, 2nd, Afshari CA, and Hamadeh HK (2013) A multifactorial approach to hepatobiliary transporter assessment enables improved therapeutic compound development. *Toxicological sciences : an official journal of the Society of Toxicology* **136:**216-241.

National Research Council (U.S.). Committee for the Update of the Guide for the Care and Use of Laboratory Animals., Institute for Laboratory Animal Research (U.S.), and National Academies Press (U.S.) (2011) Guide for the care and use of laboratory animals, pp xxv, 220 p., National Academies Press,, Washington, D.C.

Olson H, Betton G, Robinson D, Thomas K, Monro A, Kolaja G, Lilly P, Sanders J, Sipes G, Bracken W, Dorato M, Van Deun K, Smith P, Berger B, and Heller A (2000) Concordance of the toxicity of pharmaceuticals in humans and in animals. *Regul Toxicol Pharmacol* **32:**56-67.

Ryan JC, Dunn KW, and Decker BS (2014) Effects of chronic kidney disease on liver transport: quantitative intravital microscopy of fluorescein transport in the rat liver. *Am J Physiol Regul Integr Comp Physiol* **307:**R1488-1492.

Stieger B, Meier Y, and Meier PJ (2007) The bile salt export pump. *Pflugers Arch* **453:**611-620.

Swift B, Pfeifer ND, and Brouwer KL (2010) Sandwich-cultured hepatocytes: an in vitro model to evaluate hepatobiliary transporter-based drug interactions and hepatotoxicity. *Drug Metab Rev* **42:**446-471.

van Staden CJ, Morgan RE, Ramachandran B, Chen Y, Lee PH, and Hamadeh HK (2012) Membrane vesicle ABC transporter assays for drug safety assessment. *Curr Protoc Toxicol* **Chapter 23:**Unit 23 25.

Wang R, Chen HL, Liu L, Sheps JA, Phillips MJ, and Ling V (2009) Compensatory role of P-glycoproteins in knockout mice lacking the bile salt export pump. *Hepatology (Baltimore, Md* **50:**948-956.

Woodhead JL, Yang K, Siler SQ, Watkins PB, Brouwer KL, Barton HA, and Howell BA (2014) Exploring BSEP inhibition-mediated toxicity with a mechanistic model of drug-induced liver injury. *Front Pharmacol* **5:**240.

Ye ZW, Augustijns P, and Annaert P (2008) Cellular accumulation of cholyl-glycylamido-fluorescein in sandwich-cultured rat hepatocytes: kinetic characterization, transport mechanisms, and effect of human immunodeficiency virus protease inhibitors. *Drug metabolism and disposition: the biological fate of chemicals* **36:**1315-1321.

DMD Fast Forward. Published on February 21, 2018 as DOI: 10.1124/dmd.117.079277
This article has not been copyedited and formatted. The final version may differ from this version.

Figure legends

Figure 1 –Intravital microscopy of CGamF transport in the liver of a living rat – Intravital multiphoton microscopy was used to collect a series of fluorescence image volumes from the liver of a living rat following intravenous injection of 4 mg/kg CGamF. These image volumes were converted into a series of maximum projection (MIP) images for each timepoint, which are shown here. CGamF, initially appearing in the sinusoids was rapidly transported, detectible in canaliculi as early as 1 minute after infusion, and subsequently increased in concentration over the next 3 minutes. The rat was injected with Hoechst 33342 (2 mg/kg) 30 min prior to imaging to label nuclei (blue). Scale bar is 50 microns in length.

Figure 2 – Effects of AMG 009 on CGamF transport in rat liver – (A) – Time course of CGamF transport in the livers of living rats 20 minutes after IV injection with vehicle (left) 10 mg/kg AMG 009 (middle) or 30 mg/kg AMG 009 (right). Top row – projected images collected 90 seconds after infusion of CGamF. Bottom row – projected images collected 5 minutes after infusion of CGamF. The time-series of MIP images collected over 5 minutes following IV injection in rats treated with vehicle or 30 mg/kg AMG 009 is shown in an accompanying video (Supplemental Video1) (at ~100x speed). (B) – Mosaics assembled from 9 adjacent volumes collected 12-15 minutes after IV injection of CGamF for a rat treated with vehicle (left) or 30 mg/kg AMG 009 (right). Scale bars are 50 microns (A) or 100 microns (B) in length.

Figure 3 –*In vivo* dose-dependent inhibition of canalicular secretion by AMG 009 in rats - Kinetics of canalicular secretion of CGamF for individual rats treated with vehicle (A), 3 mg/kg AMG 009 (B), 10 mg/kg AMG 009 (C) or 30 mg/kg AMG 009 (D). In each graph measurements

are shown for each of three replicate rats. (The small spike in fluorescence at 1 min is an artifact of the segmentation procedure, which detects a small fraction of the sinusoid fluorescence during infusion.) (E) – Summary of effects on CGamF net secretion rate (linear rate of initial secretion). (Means ± standard error of the mean). * - P < .05, Dunnett's multiple comparison procedure. N = 3 for all conditions.

Figure 4 – Quantification of the *in vivo* effects of AMG 009 on hepatocellular CGamF uptake - Kinetics of CGamF cytosolic uptake for individual rats treated with vehicle (A), 3 mg/kg AMG 009 (B), 10 mg/kg AMG 009 (C) or 30 mg/kg AMG 009 (D). In each graph measurements are shown for each of three replicate rats. (E) – Summary of effects on CGamF net uptake (linear rate during initial uptake). (F) - Cumulative cytosolic CGamF fluorescence, measured from 6-11 minutes after CGamF injection. (Means ± standard error of the mean). N = 3 for all conditions.

Figure 5 – Effects of AMG 009 on CLF transport in rat liver – Time course of CLF transport in the livers of living rats 20 minutes after IV injection with vehicle (left) or 30 mg/kg AMG 009 (right). The time-series of MIP images collected over 5 minutes following IV injection in rats treated with vehicle or 30 mg/kg AMG 009 is shown in an accompanying video (Supplemental Video2) (at ~100x speed). Scale bar is 50 microns in length.

Figure 6 – Quantification of the effects of AMG 009 on CLF transport *in vivo* – (A) Kinetics of CLF canalicular secretion for individual rats treated with vehicle (black symbols) or 30 mg/kg AMG 009 (red symbols). Measurements are shown for each of three replicate rats for each condition. (B) Summary of effects on rates of CLF net secretion (linear rate of initial secretion). (Means ± standard error of the mean). (C) Kinetics of cytosolic CLF uptake for individual rats treated with vehicle (black symbols) or 30 mg/kg AMG 009 (red symbols). Measurements are

shown for each of three replicate rats for each condition. (D) – Summary of effects on net CLF uptake (linear rate during initial uptake). (Means ± standard error of the mean). * - P < .05, Students t-test. N = 3 for all conditions.

Figure 7 – Serum total bile acids in rats following a single IV dose of AMG 009. Serum total bile acid levels in rats treated IV with vehicle, 10, 30, or 100 mg/kg AMG 009 over a 24 hr time course. Three rats per time point, per dose group. Symbols represent mean values at each time point, and bars are SEM. *Dunnett's post hoc comparison, $p < 0.05$ (performed in GraphPad Prism 7).

Figure 8 –Effects of bosentan on CGamF transport in rat liver – (A) – Time course of CGamF transport in the liver of living rats 20 minutes after IV injection with vehicle (left) 10 mg/kg bosentan (middle) or 30 mg/kg bosentan (right). Top row – projected images collected 90 seconds after CGamF infusion. Bottom row – projected images collected 5 minutes after CGamF infusion. The time-series of MIP images collected over 5 minutes following IV injection in rats treated with vehicle or 30 mg/kg bosentan is shown in an accompanying video (Supplemental Video3) (at ~100x speed). (B) – Mosaics assembled from 9 adjacent volumes collected 12-15 minutes after IV injection of CGamF for a rat treated with vehicle (left) or 30 mg/kg bosentan (right). Scale bars are 50 microns (A) or 100 microns (B) in length.

Figure 9 –*In vivo* dose-dependent inhibition of canalicular secretion by bosentan in rats - Kinetics of canalicular CGamF secretion for individual rats treated with vehicle (A), 3 mg/kg bosentan (B), 10 mg/kg bosentan (C) or 30 mg/kg bosentan (D). In each graph measurements are shown for each of three replicate rats, except the 3 mg/kg treatment group for which one animal was omitted due to lack of detectible bosentan in plasma. (E) – Summary of effects on the rate of net CGamF secretion (linear rate during initial secretion). (Means ± standard error of

DMD Fast Forward. Published on February 21, 2018 as DOI: 10.1124/dmd.117.079277
This article has not been copyedited and formatted. The final version may differ from this version.

the mean). * - P < .05, ** - P < .01, Dunnett's multiple comparison procedure. N = 3 for all conditions, except the 3 mg/kg treatment group for which one animal was omitted due to lack of detectible bosentan in plasma.

Figure 10 –Quantification of the *in vivo* effects of bosentan on CGamF hepatocellular uptake - Kinetics of cytosolic CGamF uptake for individual rats treated with vehicle (A), 3 mg/kg bosentan(B), 10 mg/kg bosentan (C) or 30 mg/kg bosentan (D). In each graph measurements are shown for each of three replicate rats, except the 3 mg/kg treatment group for which one animal was omitted due to lack of detectible bosentan in plasma. (E) – Summary of effects on net CGamF uptake (linear rate during initial uptake). (F) - Cumulative cytosolic CGamF fluorescence, measured from 6-11 minutes after injection of CGamF. (Means ± standard error of the mean). * - P < .05, Dunnett's multiple comparison procedure. N = 3 for all conditions, except the 3 mg/kg treatment group for which one animal was omitted due to lack of detectible bosentan in plasma.

Figure 11 –Effects of bosentan on CLF transport in rat liver – Time course of CLF transport in the livers of living rats 20 minutes after IV injection with vehicle (left) or 30 mg/kg bosentan (right). The time-series of MIP images collected over 5 minutes following IV injection in rats treated with vehicle or 30 mg/kg bosentan is shown in an accompanying video (Supplemental Video4) (at ~100x speed). Scale bar is 50 microns in length.

Figure 12 – Quantification of the effects of bosentan on CLF transport *in vivo* – (A) Kinetics of canalicular CLF secretion for individual rats treated with vehicle (black symbols) or 30 mg/kg bosentan (red symbols). Measurements are shown for each of three replicate rats for each condition. (B) Summary of effects on rates of net CLF secretion (linear rate of initial secretion). (Means ± standard error of the mean). (C) Kinetics of cytosolic CLF uptake for

individual rats treated with vehicle (black symbols) or 30 mg/kg bosentan (red symbols). Measurements are shown for each of three replicate rats for each condition. (D) – Summary of effects on net CLF uptake (linear rate during initial uptake). (Means ± standard error of the mean). ** - P < .01, Students t-test. N = 3 for all conditions.

Figure 13 – Serum total bile acids in rats following a single IV dose of bosentan. Serum total bile acid levels in rats treated IV with vehicle, 10, 30, or 100 mg/kg bosentan over a 24 hr time course. Three rats per time point, per dose group. Symbols represent mean values at each time point, and bars are SEM. *Dunnett's post hoc comparison, $p < 0.05$ (performed in GraphPad Prism 7).

DMD Fast Forward. Published on February 21, 2018 as DOI: 10.1124/dmd.117.079277
This article has not been copyedited and formatted. The final version may differ from this version.

Tables

Table 1 - Summary of intravital microscopy measurements

		Net canalicular secretion rate (AUs/min)		9-field canalicular fluorescence (AUs)	Cytosolic uptake rate (AUs/min)		Cumulative cytosolic exposure (AUs)		9-field cytosolic fluorescence (AUs)
		CGamF	**CLF**	**CGamF**	**CGamF**	**CLF**	**CGamF**	**CLF**	**CGamF**
AMG 009	**Vehicle**	5.426e+06 ± 1.301e+06	2.104e+07 ± 6.176e+06	1.1870e+08 ± 5.321e+07	180.7 ± 29.17	135.9 ± 7.217	4765 ± 550.3	2787.8 ± 505.4	587.5 ± 21.50
	3 mg/kg	2.057e+06 ± 1.701e+06	ND	4.455e+07 ± 1.457e+07	154.0 ± 17.42	ND	4143 ± 623.2	ND	598.3 ± 24.29
	10 mg/kg	3.273e+05 ± 52250 *	ND	2.873e+07 ± 7.516e+06 *	180.6 ± 7.160	ND	5663 ± 469.5	ND	662.0 ± 18.58
	30 mg/kg	-1.1612e+05 ± 82430 *	27870 ± 25380 *	2.733e+06 ± 7.694e+05 *	140.5 ± 10.86	68.90 ± 14.95*	4283 ± 1000.	3450 ± 897.6	568.7 ± 13.67
Bosentan	**Vehicle**	1.238e+07 ± 1.816e+06	1.622e+07 ± 1.189e+06	1.839e+08 ± 3.380e+07	248.80 ± 22.96	143.40 ± 7.538	5007 ± 450.7	2809 ± 164.9	512.0 ± 12.70
	3 mg/kg	9.950e+06 ± 1.453e+06	ND	1.687e+08 ± 4.719e+07	148.90 ± 58.61	ND	2882 ± 412.9	ND	470.0 ± 3.000
	10 mg/kg	6.854e+06 ± 6.057e+05 *	ND	1.120e+08 ± 2.719e+06	137.6 ± 31.12	ND	3878 ± 993.2	ND	474.0 ± 5.292
	30 mg/kg	2.555e+06 ± 9.804e+05 **	4.681e+06 ± 2.182e+06 **	1.039e+08 ± 1.180e+07	128.5 ± 7.611 *	57.62 ±10.75**	5110 ± 623.4	3683 ± 489.7	503.7 ± 14.35

ND – not determined

** - P < .05, ** - P < .01, Dunnett's multiple comparison, Students t-test for single comparisons. N = 3 for all conditions, except the 3 mg/kg bosentan treatment group (CGamF studies) for which one animal was omitted due to lack of detectible bosentan in plasma and the 9-field integrated CGamF measures in vehicle treated rats in the AMG009 studies, for which mosaics were collected for only 2 rats.*

DMD Fast Forward. Published on February 21, 2018 as DOI: 10.1124/dmd.117.079277
This article has not been copyedited and formatted. The final version may differ from this version.

Table 2 – Estimated drug exposure for the intravital imaging studies

Compound	Dose (mg/kg)	Fluorescent Probe	Subject	Plasma (µg/L)	Estimated C_{max} (µg/L)	Estimated C_{max} (µM)	Mean Estimated C_{max} (µM)
AMG 009	3	CGamF	8	1970	3500	6	11
			9	3240	5700	10	
			10	5280	9200	16	
	10	CGamF	11	28600	50000	86	74
			12	25000	44000	76	
			13	20200	35000	60	
	30	CGamF	14	120000	210000	360	510
			15	191000	330000	570	
			16	195000	340000	590	
	30	CLF	17	177000	310000	530	430
			18	135000	240000	410	
			19	115000	200000	350	
Bosentan	3	CGamF	1	BQL	-	-	6.3
			2	1340	1900	3.4	
			3	3650	5100	9.2	
	10*	CGamF	4	15700	22000	40	37
			5	13800	19000	34	
	30*	CGamF	6	41100	58000	110	170
			7	86700	120000	220	
	30	CLF	20	59800	84000	150	210
			21	101000	140000	250	
			22	88400	120000	220	

*Exposure of AMG 009 or bosentan during the intravital imaging studies, and an estimated C_{max} based on previously conducted IV studies with these compounds. As shown in this table, subject number 1 in the 3 mg/kg bosentan dose group had no measurable exposure (limit of quantitation was 100 µg/L). Given that the other two animals in this dose group had plasma concentrations 13 – 36x the limit of quantitation, it was concluded that subject number 1 was not properly dosed and imaging data for this animal was removed from the dataset. Formula weight for AMG 009 is 581.47, and for bosentan is 551.62. BQL = below the quantitation limit. *Blood was not collected for exposure analysis for one animal in each of the 10 and 30 mg/kg bosentan groups.*

DMD Fast Forward. Published on February 21, 2018 as DOI: 10.1124/dmd.117.079277
This article has not been copyedited and formatted. The final version may differ from this version.

Table 3 - Estimated C_{max}/transporter IC_{50} ratios relative to effects on total serum bile acid levels versus intravital imaging.

Compound	Dose level (mg/kg)	C_{max} (µM, total drug)	C_{max}/Bsep IC_{50} ratio	C_{max}/Mrp2 IC_{50} ratio	Significant effect on:		
					Serum total bile acids	Net rate of CGamF canalicular secretion	Net rate of CLF canalicular secretion
AMG 009	3	11	0.48	0.27	NT	No	NT
	10	74	3.2	1.8	No	Yes	NT
	30*	470	20	11	No	Yes	Yes
	100**	1010	44	25	Yes	NT	NT
Bosentan	3	6.3	0.15	NC	NT	No	NT
	10	37	0.90	NC	No	Yes	NT
	30*	190	4.6	NC	Yes	Yes	Yes
	100**	390	9.50	NC	Yes	NT	NT

*Plasma was collected 50 minutes post IV dose of AMG 009 or bosentan during the intravital imaging studies. C_{max} values were estimated for the intravital studies by comparing the 50 minute plasma concentrations to comparable time points from previously conducted pharmacokinetic studies in rats with AMG 009 or bosentan. *Estimated C_{max} is the mean value for the CGamF and CLF experiments. **Actual mean C_{max} values from the previous studies conducted by Amgen. BQL = below the quantitation limit, NC = not calculated, NT = not tested.*

DMD Fast Forward. Published on February 21, 2018 as DOI: 10.1124/dmd.117.079277
This article has not been copyedited and formatted. The final version may differ from this version.

Figures

DMD Fast Forward. Published on February 21, 2018 as DOI: 10.1124/dmd.117.079277
This article has not been copyedited and formatted. The final version may differ from this version.

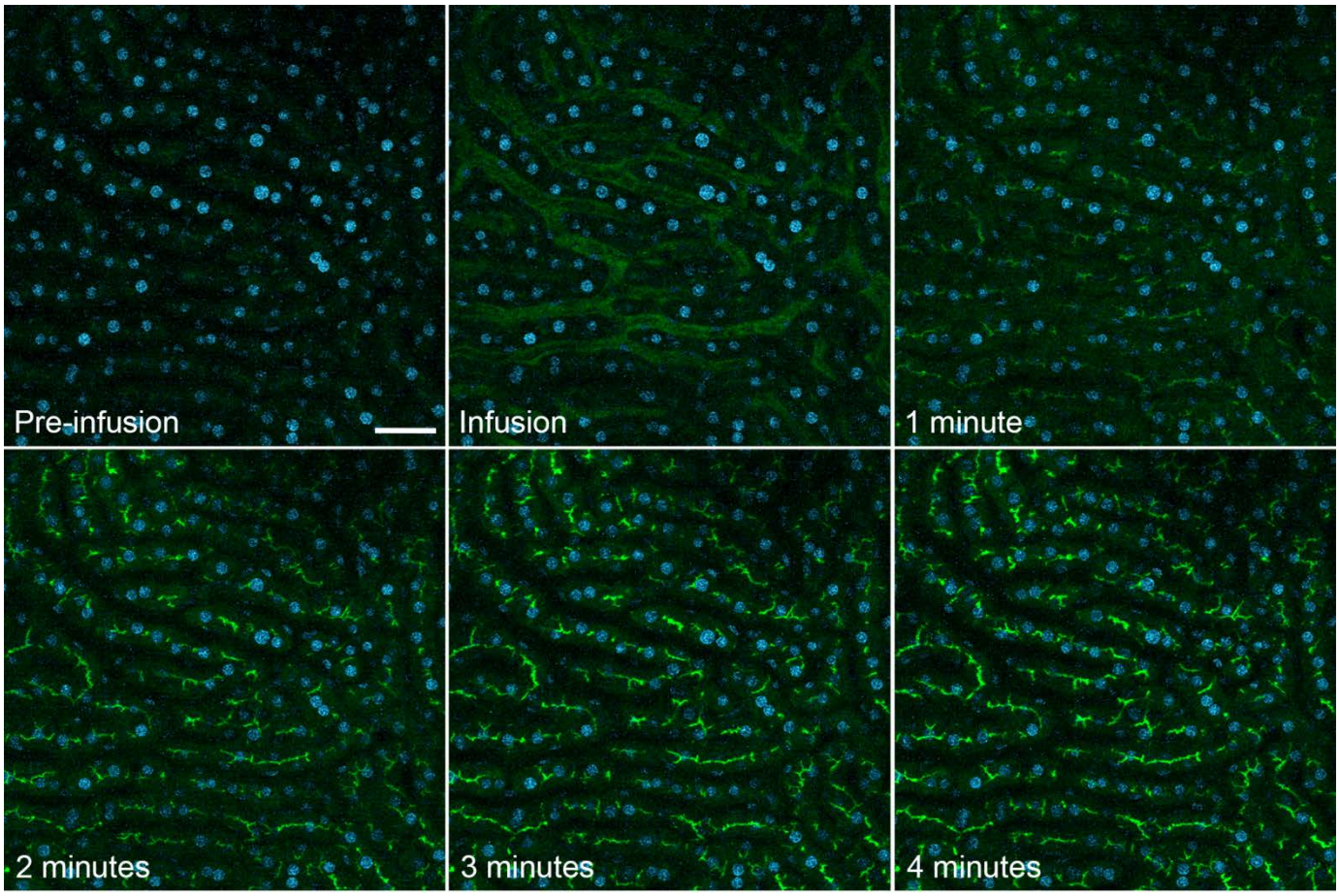

Figure 1

DMD Fast Forward. Published on February 21, 2018 as DOI: 10.1124/dmd.117.079277
This article has not been copyedited and formatted. The final version may differ from this version.

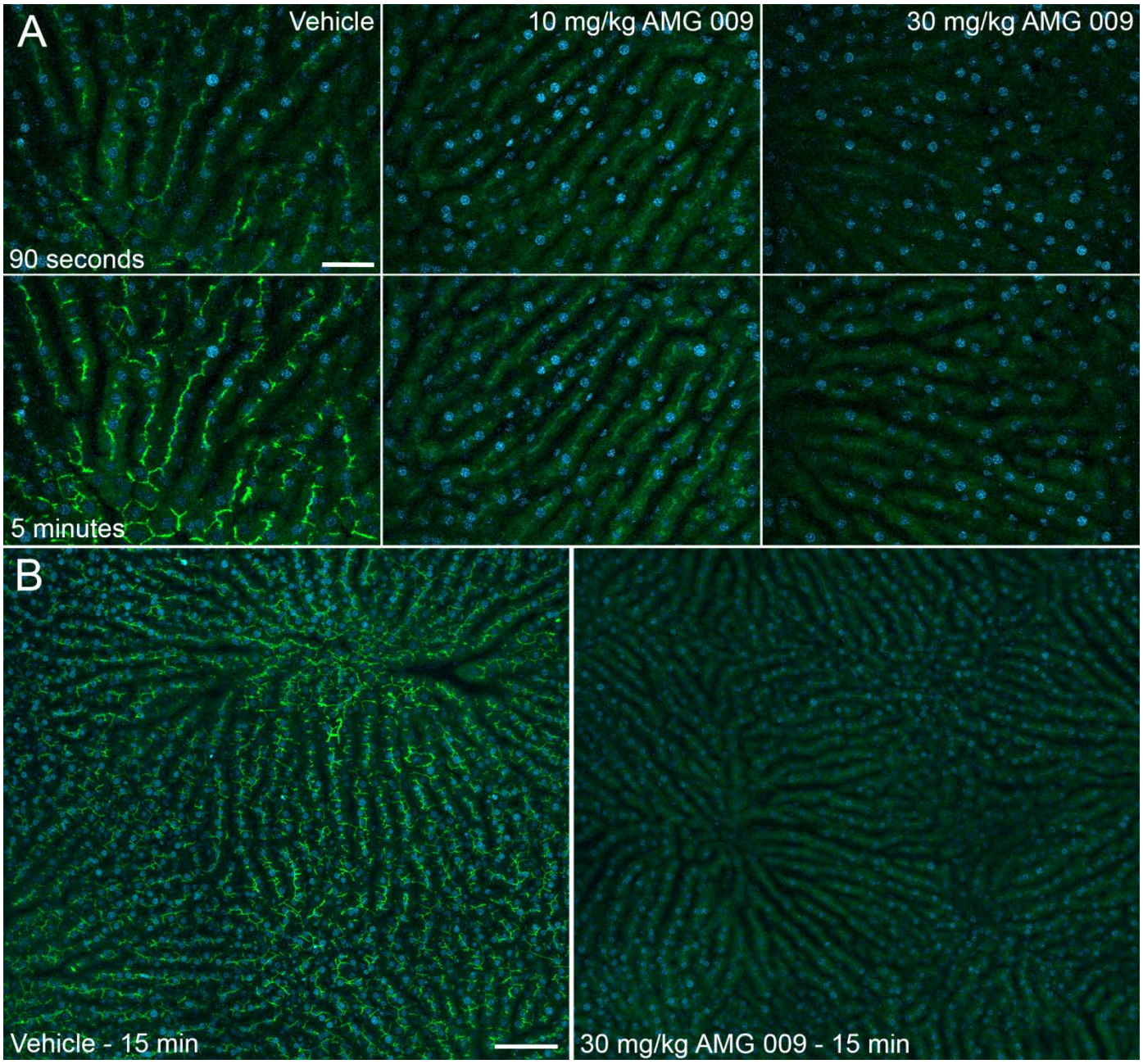

Figure 2

DMD Fast Forward. Published on February 21, 2018 as DOI: 10.1124/dmd.117.079277
This article has not been copyedited and formatted. The final version may differ from this version.

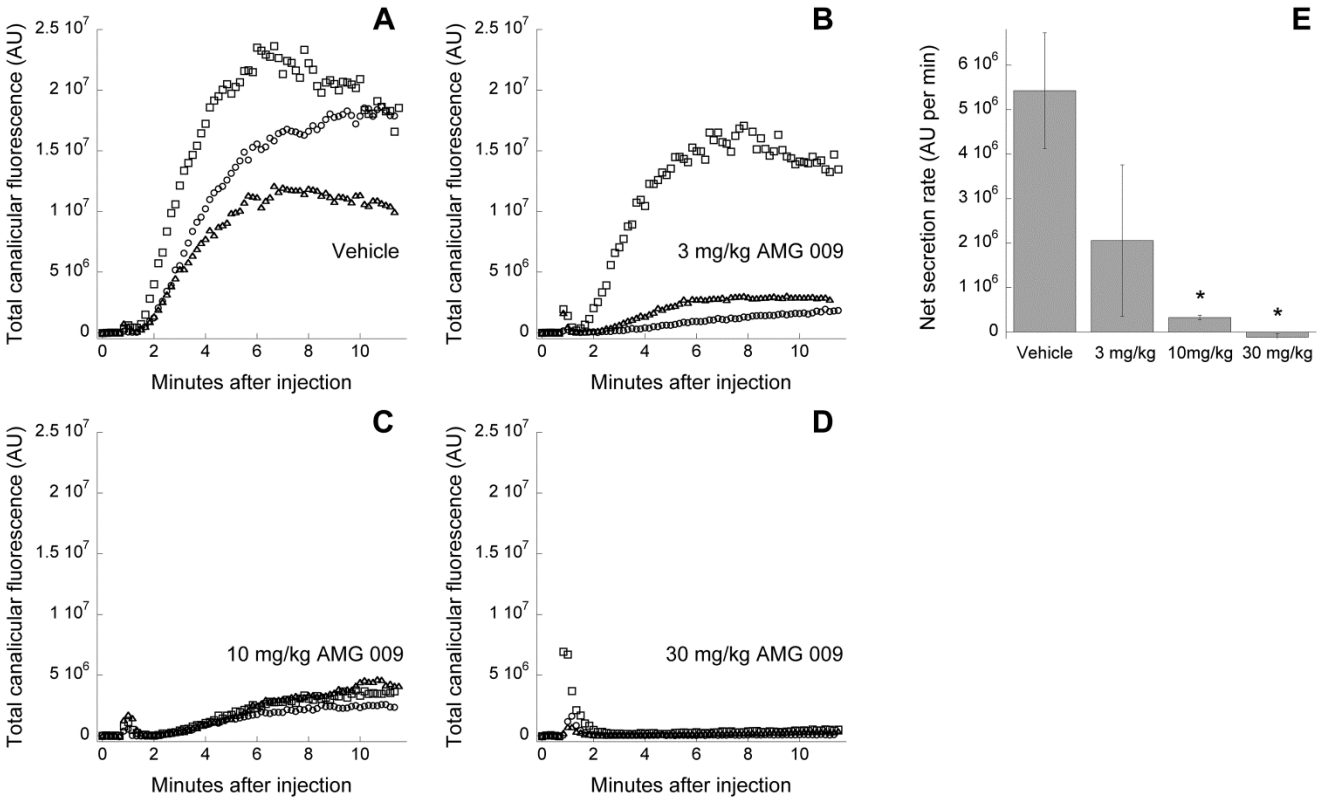

Figure 3

DMD Fast Forward. Published on February 21, 2018 as DOI: 10.1124/dmd.117.079277
This article has not been copyedited and formatted. The final version may differ from this version.

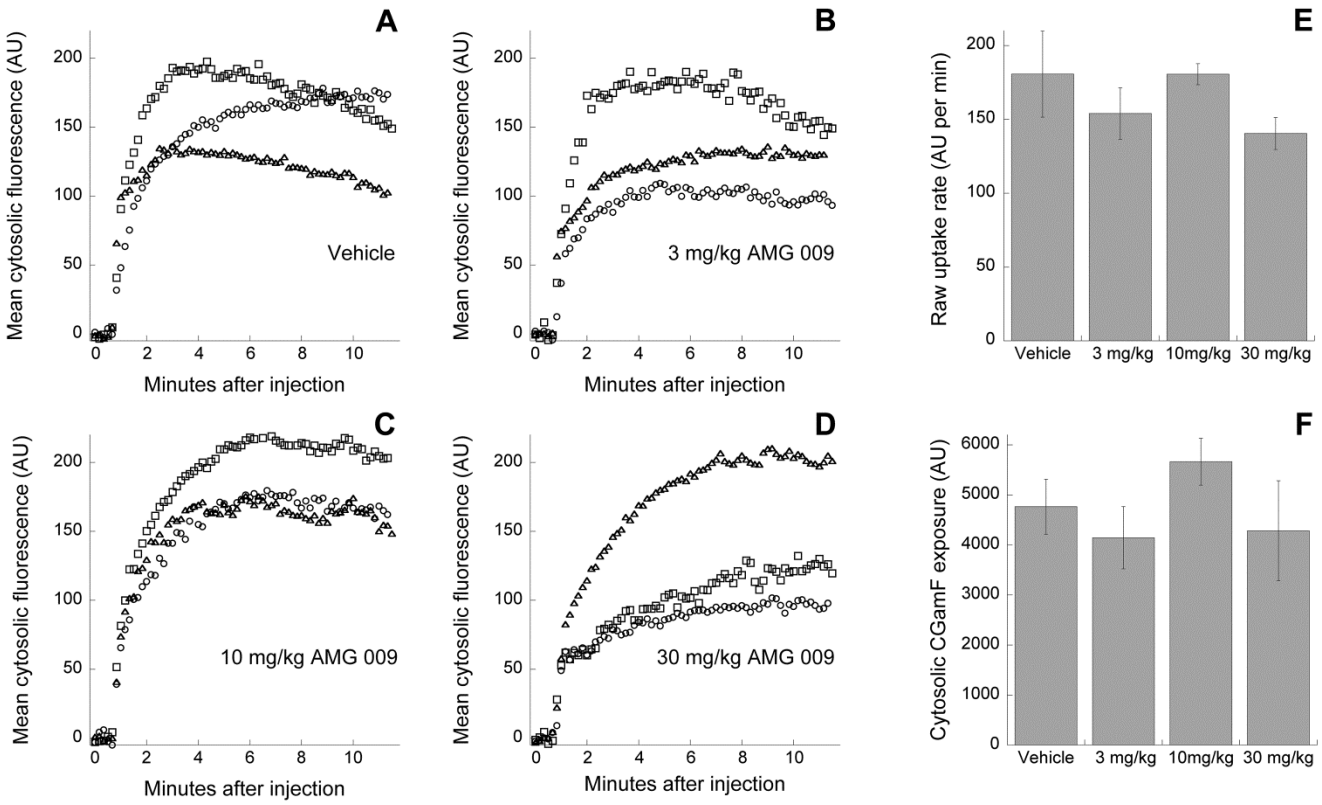

Figure 4

DMD Fast Forward. Published on February 21, 2018 as DOI: 10.1124/dmd.117.079277
This article has not been copyedited and formatted. The final version may differ from this version.

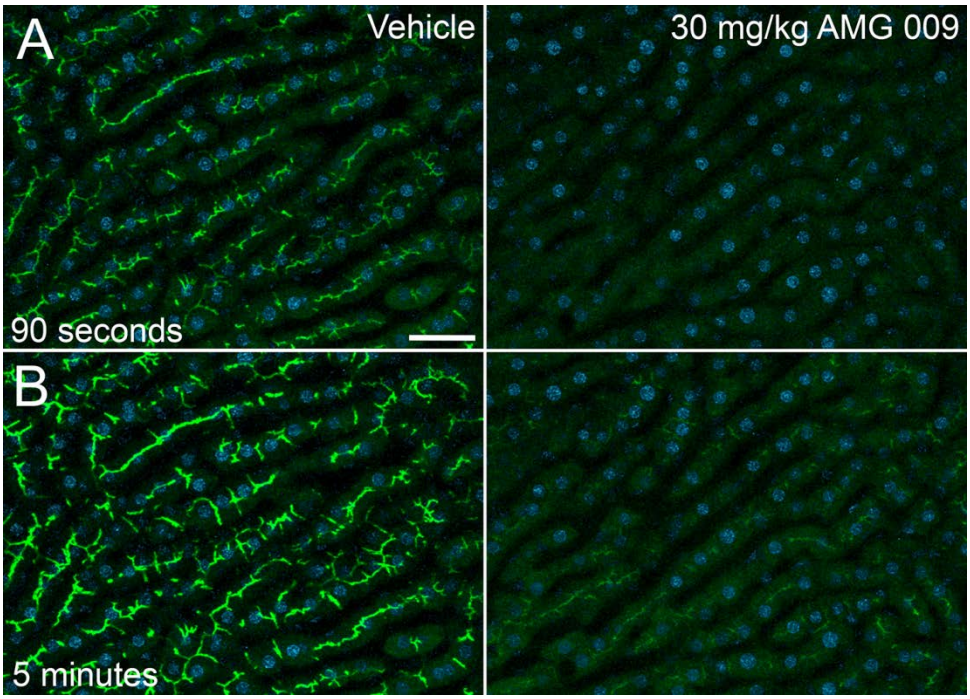

Figure 5

DMD Fast Forward. Published on February 21, 2018 as DOI: 10.1124/dmd.117.079277
This article has not been copyedited and formatted. The final version may differ from this version.

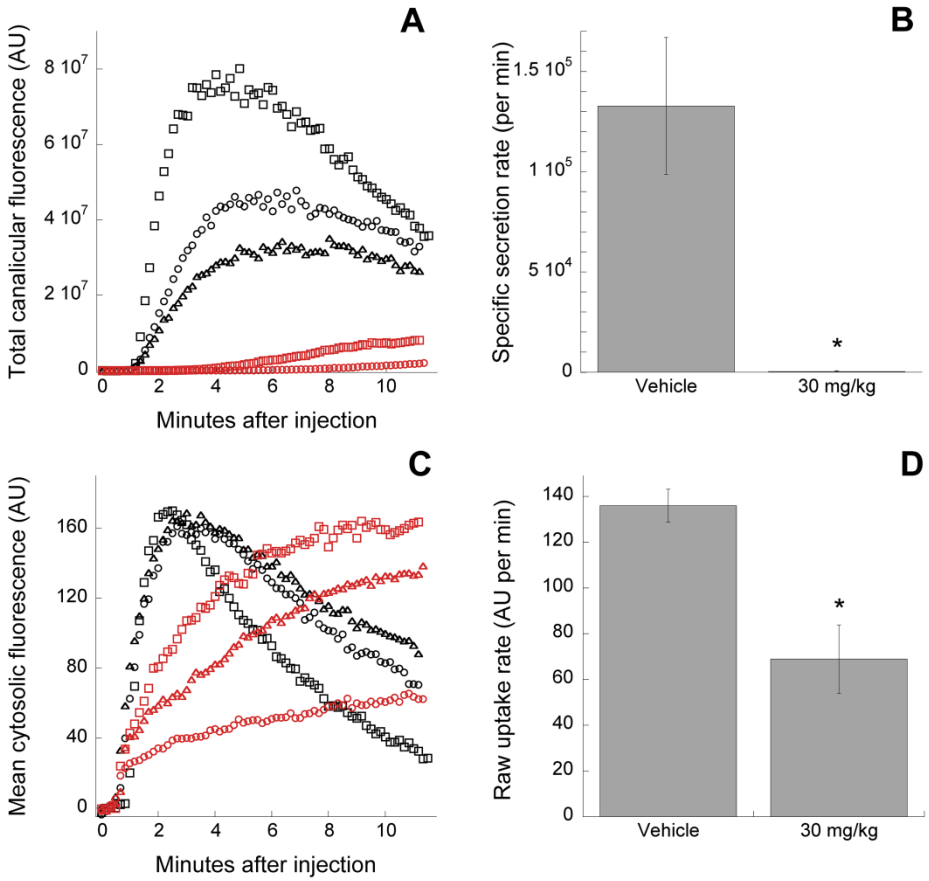

Figure 6

DMD Fast Forward. Published on February 21, 2018 as DOI: 10.1124/dmd.117.079277
This article has not been copyedited and formatted. The final version may differ from this version.

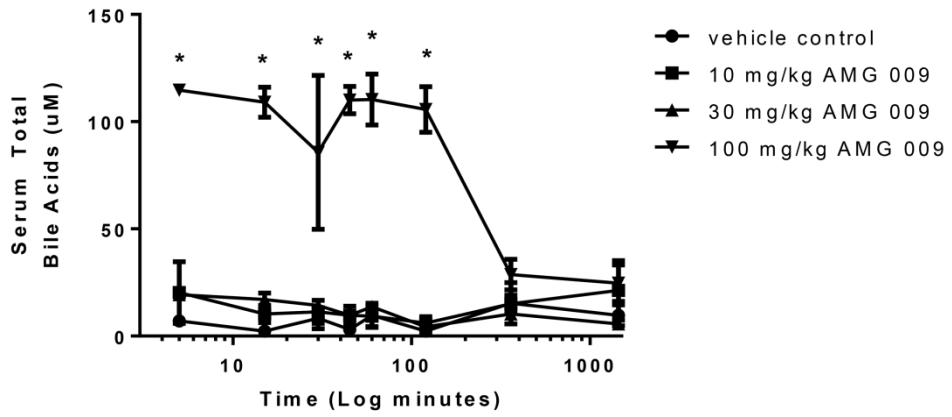

Figure 7

DMD Fast Forward. Published on February 21, 2018 as DOI: 10.1124/dmd.117.079277
This article has not been copyedited and formatted. The final version may differ from this version.

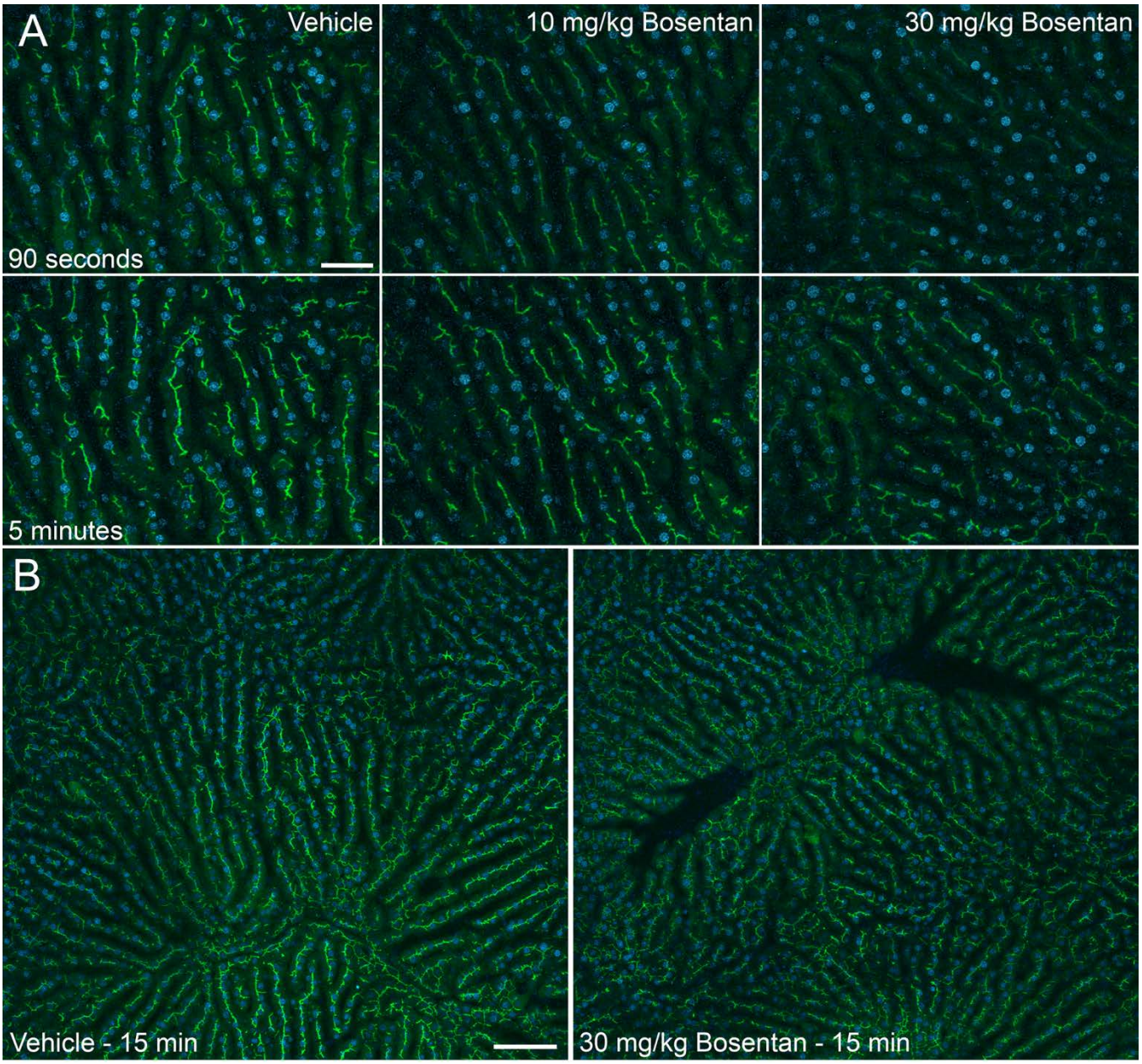

Figure 8

DMD Fast Forward. Published on February 21, 2018 as DOI: 10.1124/dmd.117.079277
This article has not been copyedited and formatted. The final version may differ from this version.

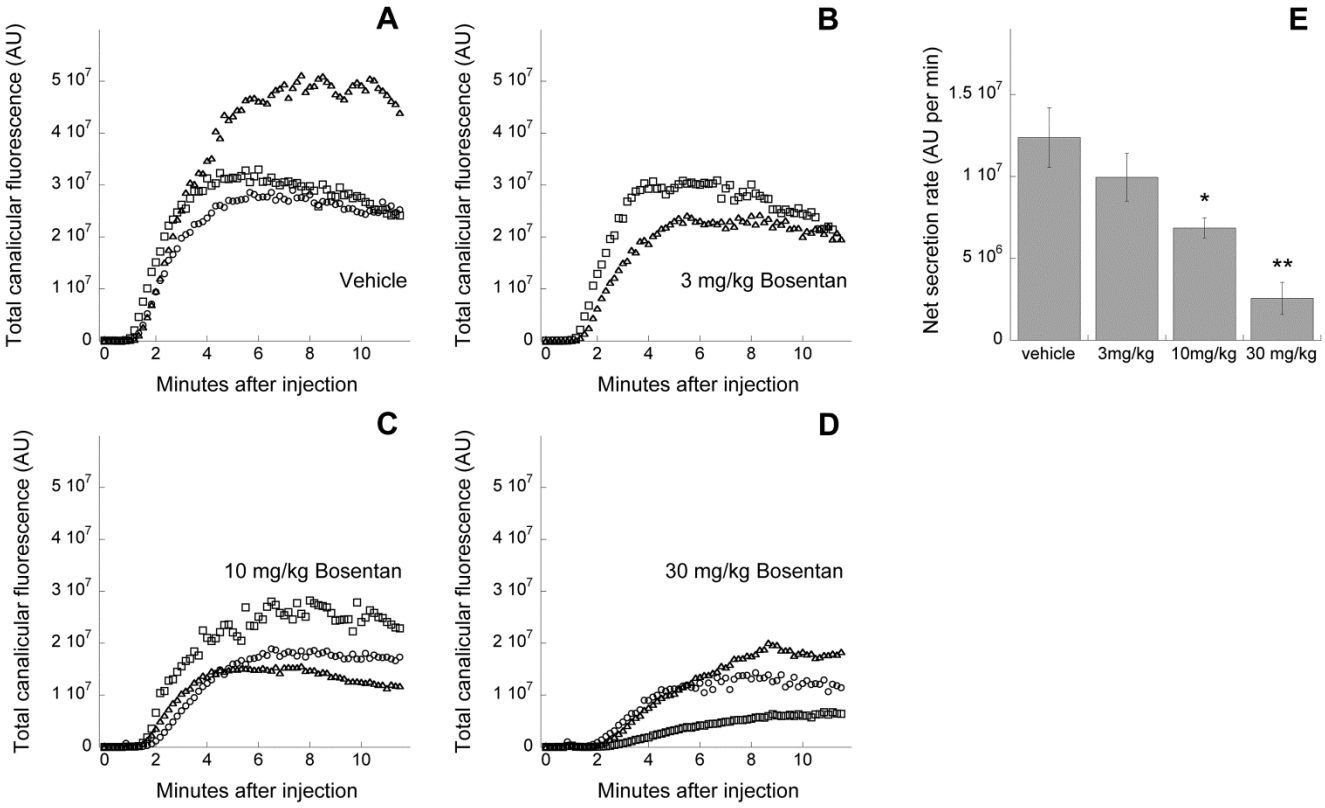

Figure 9

DMD Fast Forward. Published on February 21, 2018 as DOI: 10.1124/dmd.117.079277
This article has not been copyedited and formatted. The final version may differ from this version.

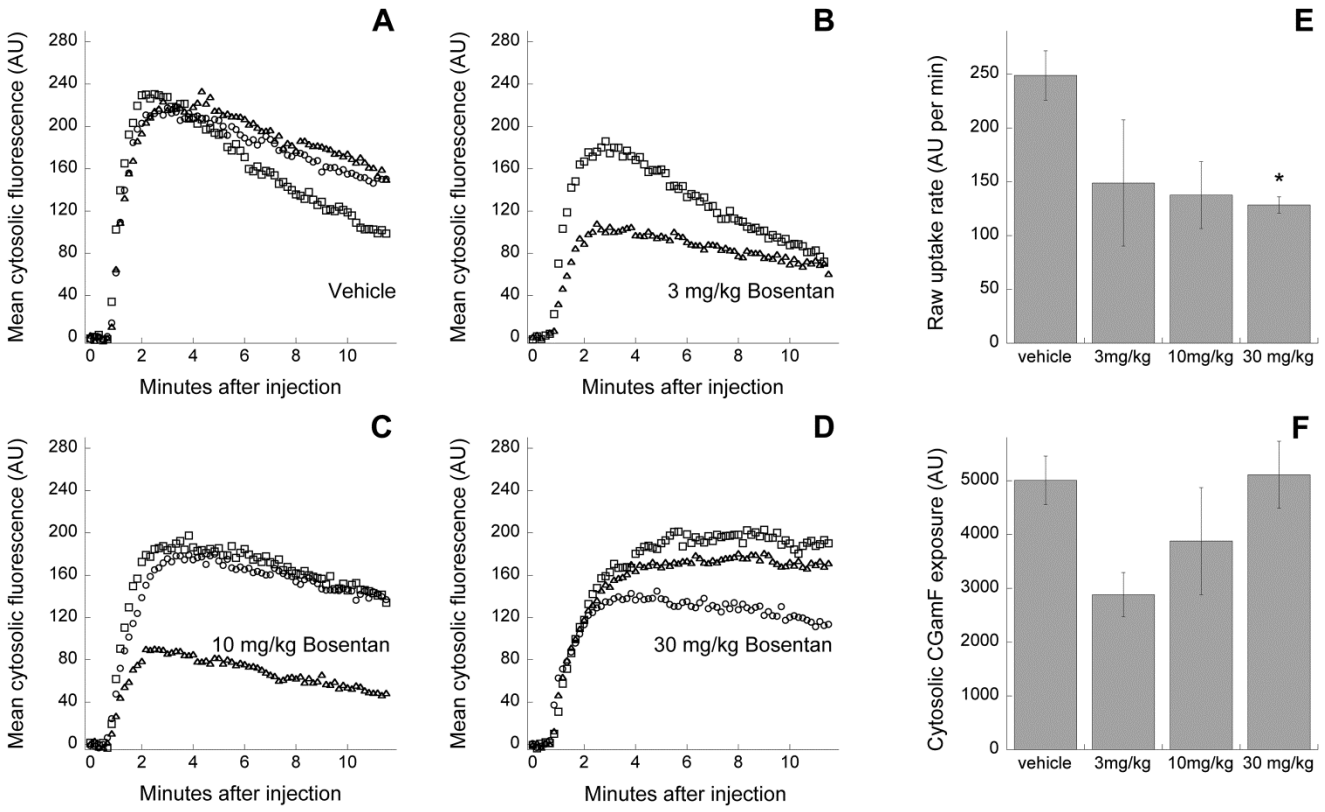

Figure 10

DMD Fast Forward. Published on February 21, 2018 as DOI: 10.1124/dmd.117.079277
This article has not been copyedited and formatted. The final version may differ from this version.

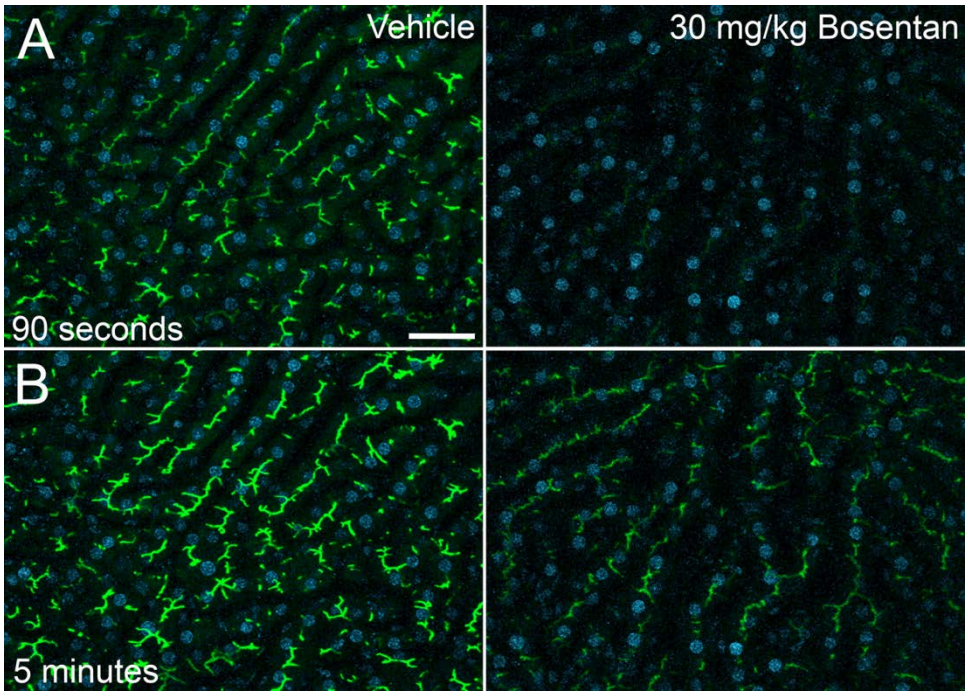

Figure 11

DMD Fast Forward. Published on February 21, 2018 as DOI: 10.1124/dmd.117.079277
This article has not been copyedited and formatted. The final version may differ from this version.

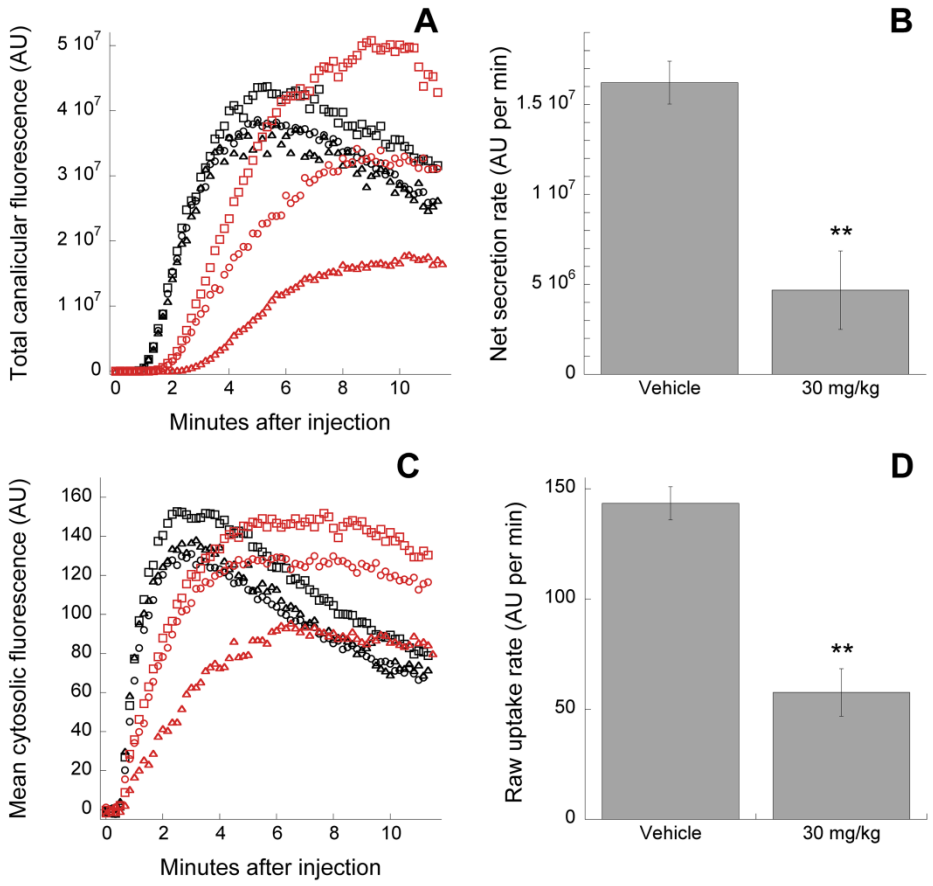

Figure 12

DMD Fast Forward. Published on February 21, 2018 as DOI: 10.1124/dmd.117.079277
This article has not been copyedited and formatted. The final version may differ from this version.

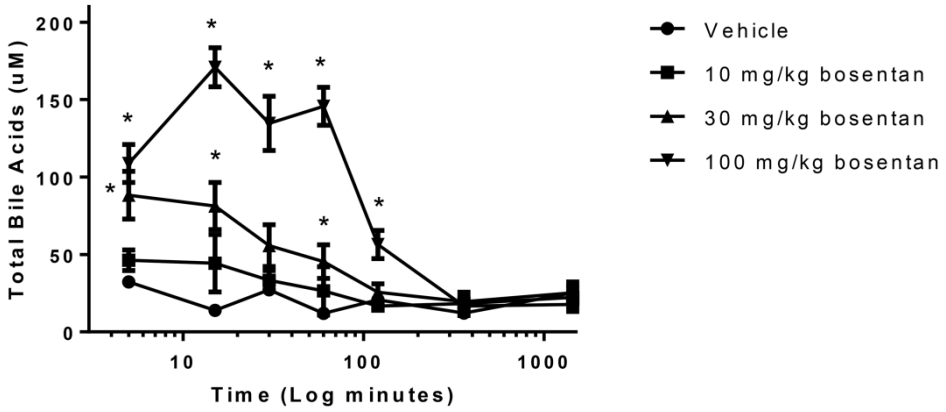

Figure 13